

Do superfluid instabilities prevent neutron star precession?

K. Glampedakis¹, N. Andersson² & D.I. Jones²

¹ *SISSA/International School for Advanced Studies and INFN, via Beirut 2-4, 34014 Trieste, Italy*

² *School of Mathematics, University of Southampton, Southampton SO17 1BJ, UK*

31 October 2018

ABSTRACT

We discuss short wavelength (inertial wave) instabilities present in the standard two-fluid neutron star model when there is sufficient relative flow along the superfluid neutron vortex array. We demonstrate that these instabilities may be triggered in precessing neutron stars, since the angular velocity vectors of the neutron and proton fluids are misaligned during precession. The presence of such an instability would render the standard, solid body rotation, model for free precession inconsistent. Our results suggest that the standard (Eulerian) slow precession that results for weak drag between the vortices and the charged fluid (protons and electrons) is not seriously constrained by the existence of the instability. In contrast, the fast precession, which results when vortices are strongly coupled to the charged component, is generally unstable. This implies that fast precession may not be realised in astrophysical systems.

1 INTRODUCTION

Over the last few years, the modelling of neutron star free precession has attracted considerable attention from theorists. This has been caused in large part by the reported observations of free precession in PSR B1828-11 by Stairs, Lyne & Shemar (2000). There exist several other precession candidates, most notably PSR B1642-03 (Shabanova, Lyne & Urama 2001), but none are as convincing as PSR B1828-11, whose pulse variations extend over multiple precession periods and are visible in multiple channels (pulse time-of-arrival and beam shape).

This precessional motion is of great interest in several regards. Firstly, PSR B1828-11 is the only clear precession candidate out of the several thousand known pulsars, which begs the questions why is precession so rare, and what has set PSR B1828-11 into precession in the first place? Secondly, the free precession timescale as extracted from the observations is approximately 500 days (modulo a possible factor of two up or down, depending on which of the observed harmonics in the frequency spectrum is the fundamental one). This is extremely uncomfortable from the theoretical point of view, as the canonical model of a neutron star containing one or more superfluid components would suggest a much shorter precession timescale. Instead, this long period free precession period seems to be consistent with the simple wobble of a star deformed away from sphericity by strains in its crust or by a magnetic field, with superfluidity playing no role whatsoever (Akgün, Link & Wasserman 2006). It is this second question regarding the apparent lack of the effects of superfluidity with which we will mainly be concerned in this paper.

The basic picture is as follows. Both on theoretical grounds, and in order to explain the glitch phenomena, neutron stars are believed to contain superfluid components

whose rotation is achieved by their forming arrays of vortices pointing along the rotation axis. In a pioneering paper Shaham (1977) showed that in the limit where these vortices attach or ‘pin’ themselves tightly to the radio-emitting crustal phase (as is required to explain the glitches), the classical free precession of the star is greatly modified by the gyroscopic effect of the superfluid, whose angular momentum vector would be fixed in the crust’s frame. The resulting free precession period is then approximately $P/(I_s/I_1 + \epsilon)$, where P is the spin period, I_s and I_1 the moments of inertia of the superfluid and crustal phases, and ϵ the dimensionless non-sphericity in the crust’s moment of inertia tensor. Note that by ‘crust’ we really mean the crystalline crust itself and any other part of the star coupled to it on sufficiently short timescale to participate in its precession, which probably includes the core proton fluid.

One region where neutron vortices are expected to interact strongly with the crust is the *inner crust*, where neutron and crustal matter coexist. The interaction here is expected to be sufficiently strong that the vortices pin tightly to the crustal lattice, resulting in a very short free precession period, in conflict with the PSR 1828-11 observations. A possible resolution to this problem was suggested by Link & Cutler (2002), who argued that forces created by the precessional motion itself would un-pin the vortices, restoring long period free precession, consistent with the observations. More problematically, neutron vortices in the *core* of the neutron star are also expected to interact with the charged component. Specifically, the interior magnetic field is composed of a large number of fluxtubes (a consequence of the protons being condensed in a type-II superconductor), which can interact with the vortices via a process known as *mutual friction*. As was shown in detail by Sedrakian, Wasserman & Cordes (1999), even if this cou-

arXiv:0801.4638v1 [astro-ph] 30 Jan 2008

pling force isn't strong enough to completely pin the vortices, the free precession timescale in the coupled system is likely to be much shorter than the observed precession timescale. The significance of this result was emphasised recently by Link (2003), who argued that the observed slow precession necessitated a profound change in our view of neutron star interiors, requiring either that one or other (or both) of the posited superfluid/superconducting phases do not exist, or else that there are no regions in the interior where they exist simultaneously, perhaps because the protons form a type-I superconductor.

It is this line of argument we address in this paper. The results outlined above, leading to the prediction of fast precession, have all relied implicitly on treating the superfluid and non-superfluid phases as rigid bodies, each with a well defined angular velocity vector. However, in reality the phases are better described by the fluid Euler equations, the ansatz of rigidity having been made mainly for reasons of tractability. In this paper, which expands on initial results discussed by Glampedakis, Andersson & Jones (2007), we demonstrate that the relative motion between the two phases that rigid body free precession generates can give rise to a superfluid two-stream instability. The instability itself occurs in the inertial modes of the rotating fluids, and is related to the experimentally observed instability of Helium II explained long ago by Glaberson and collaborators (Glaberson, Johnson & Ostermeier 1974). It is also intimately linked to the neutron star instability described very recently by Sidery, Andersson & Comer (2007). As we will argue in detail, this instability renders the free precession rigid rotation ansatz inconsistent and makes all subsequent conclusions concerning the interior composition of neutron stars unsafe.

The plan of this paper is as follows. In Section 2 we describe the basic formulation of the two-fluid coupled system. Section 3 provides the plane-wave analysis and the instability criteria for inertial modes in various regimes. In Section 4 we discuss the relevance of these results for freely precessing neutron stars. The detailed precession modes are analysed in Appendix A drawing heavily on the previous work of Sedrakian, Wasserman & Cordes (1999). Our conclusions can be found in Section 5.

2 FORMULATION

When viewed as a multifluid system, a neutron star core can be modelled (at the simplest level) as a mixture of superfluid neutrons and a conglomerate of superconducting protons and normal electrons. In this picture it is assumed that the charged components are electromagnetically coupled on a timescale which is short compared to the dynamics that is being investigated. The charged plasma then forms a charge neutral fluid, which we will loosely refer to as the ‘‘protons’’ in the following. When required we will use the constituent index x , which can be either n or p , to identify the different components. A key property of the system is that the neutron and ‘‘proton’’ fluids do not flow independently with respect to each other. One of the key coupling mechanisms is the vortex mediated mutual friction, which acts dissipatively to prevent relative flow and also affects the nature of the waves in the system. The

mutual friction force appears as the result of interactions between the neutron vortices and the charged component. In the standard form, it represents scattering of electrons off of the magnetic field associated with the vortex core (Alpar, Langer & Sauls 1984; Andersson, Sidery & Comer 2006), but there may also be contributions due to the interaction between vortices and magnetic fluxtubes in the charged fluid etcetera. This latter effect may be important since the protons are expected to condense into a type II superconductor (Baym, Pethick & Pines 1969) in which the magnetic flux is carried by fluxtubes.

The smooth-averaged hydrodynamical equations for our system are (Andersson, Sidery & Comer 2006), in a rotating frame with angular velocity Ω_0^i ,

$$(\partial_t + v_n^j \nabla_j) v_i^n = \nabla_i \psi_n + 2\epsilon_{ijk} v_n^j \Omega_0^k + f_i^{\text{mf}} \quad (1)$$

$$(\partial_t + v_p^j \nabla_j) v_i^p = \nabla_i \psi_p + 2\epsilon_{ijk} v_p^j \Omega_0^k - \frac{1}{x_p} f_i^{\text{mf}} + \nu_{\text{ee}} \nabla^2 v_p^i \quad (2)$$

In these equations v_x^i are the constituent velocities and $x_p = \rho_p/\rho_n$ is the density ratio. Since it is expected that the proton to neutron ratio in the outer neutron star core where the above equations apply is about 0.05, x_p may also be taken to represent the proton fraction $\rho_p/(\rho_n + \rho_p)$. We will not be making a distinction between these quantities in the following. In the two Euler equations, the scalar functions $\psi_x = \tilde{\mu}_x + \Phi$ represent the sums of specific chemical potentials and the gravitational potential. Since our focus will be on inertial waves, we can assume that the two fluids are incompressible. This means that we also have the two continuity equations

$$\nabla_i v_x^i = 0 \quad (3)$$

In writing the above Euler equations we have made a number of simplifying assumptions. We have ignored the entrainment effect between neutrons and protons¹. We have assumed that the charged components are comoving, which when combined with an assumption of local charge neutrality, eliminates the electromagnetic Lorentz force from the equations of motion. We are also not considering the effect of vortex tension or the elasticity of the vortex array, even though quantised neutron vortices are present (in the volume averaged sense) in (1). The effect of the tension on the kinds of waves that we will study has been considered by Sidery, Andersson & Comer (2007), who found that it was generally safe to ignore it. We are also not accounting for the analogous fluxtube tension in (2).

We are, however, including the effect of shear viscosity in the equations; this is important since we will consider very short wavelength dynamics. In a superfluid neutron star core, electron-electron scattering provides the dominant contribution to the shear viscosity (Flowers & Itoh 1976; Andersson, Comer & Glampedakis 2005). This leads to the last term on the right-hand side of (2). It should

¹ Even though the entrainment, due to the strong interaction between neutrons and protons, is an important effect we ignore it in order to simplify the analysis. Its inclusion would affect the quantitative results, but should not lead to any qualitative differences. It would, of course, be interesting to study the role of entrainment in this problem at some stage.

be noted that this description is expected to be accurate at temperatures significantly below the various superfluid transition temperatures. At higher temperatures one would also have to account for various excitations, which will lead to the presence of a number of additional viscous terms (see Andersson & Comer (2006) for a discussion). In order to estimate the kinematic viscosity coefficient in (2) we use the results of Andersson, Comer & Glampedakis (2005). For a uniform density star with mass $1.4M_\odot$ and radius 10 km (our canonical values) we then find that

$$\nu_{\text{ee}} \approx 10^7 \left(\frac{10^8 \text{ K}}{T} \right)^2 \text{ cm}^2/\text{s} \quad (4)$$

The mutual friction force in (1) and (2) has the standard form (Hall & Vinen 1956; Andersson, Sidery & Comer 2006)

$$f_i^{\text{mf}} = \mathcal{B} \epsilon_{ijk} \epsilon^{kml} \hat{\omega}_n^j \omega_m^n w_l^{\text{np}} + \mathcal{B}' \epsilon_{ijk} \omega_n^j w_{\text{np}}^k \quad (5)$$

where $\omega_n^i = 2\Omega_n^i + \epsilon^{ijk} \nabla_j v_k^n$ is the neutron vorticity, the relative flow is given by $w_{\text{np}}^i = v_n^i - v_p^i$ and a ‘hat’ denotes a unit vector. This form for the mutual friction follows from assuming a resistive drag force (per unit length)

$$f_D^i = \tilde{\mathcal{R}} (v_p^i - v_L^i) \quad (6)$$

acting on each neutron vortex (moving with velocity v_L^i). Balancing the drag force against the standard Magnus force acting on the vortex leads to (5). The dimensionless coupling coefficients \mathcal{B} and \mathcal{B}' then follow from

$$\mathcal{B} = \frac{\mathcal{R}}{1 + \mathcal{R}^2}, \quad \text{and} \quad \mathcal{B}' = \frac{\mathcal{R}^2}{1 + \mathcal{R}^2} \quad (7)$$

where $\mathcal{R} = \tilde{\mathcal{R}}/\rho_n \kappa$. Here $\kappa = h/2m_n$ is the quantum of circulation. This description is quite generic. It can be taken to account for dissipative scattering of electrons off the magnetic field of the vortex core. As discussed by, for example, Andersson, Sidery & Comer (2006) this leads to a typical value of $\mathcal{B} \approx 4 \times 10^{-4}$. This means that we have

$$\mathcal{B} \approx \mathcal{R} \ll 1, \quad \mathcal{B}' \approx \mathcal{B}^2 \ll \mathcal{B} \quad (8)$$

We will refer to this as the *weak drag* limit.

However, it may well be the opposite limit that applies. Strong coupling between the neutron and proton fluids may originate from the interaction of vortices with the much more numerous magnetic fluxtubes (Sauls 1989; Ruderman, Zhu & Chen 1998; Link 2003). In this picture, each vortex is ‘‘pinned’’ to a large number of fluxtubes. As a consequence it tends to be forced to move with the proton fluid. Essentially, this additional interaction can be accounted for by modifying the drag force to

$$f_D^i = \tilde{\mathcal{R}} (v_p^i - v_L^i) + \tilde{\mathcal{R}}' (v_\phi^i - v_L^i) \quad (9)$$

where v_ϕ^i is the velocity of the fluxtubes. If we assume that the fluxtubes move with the electron/proton fluid, then it is clear that we will again end up with a mutual friction force of the form (5). Of course, this will not be the case if there is a slippage between the fluxtubes and the charged component². We will not consider this possibility here. The precise form of the drag force experienced by the vortices in

this case is not well known, but it is usually assumed that the pinning to the fluxtubes is efficient. This would mean that one would have $\tilde{\mathcal{R}}' \gg \tilde{\mathcal{R}}$ and the final mutual friction force takes the form (5) with $\mathcal{R} \approx \tilde{\mathcal{R}}'/\rho_n \kappa \gg 1$. In this case we have the *strong drag* limit,

$$\mathcal{B} \approx \frac{1}{\mathcal{R}} \ll 1, \quad 1 - \mathcal{B}' \approx \mathcal{B}^2 \ll 1 \quad (10)$$

It is worth noting that some constraints on the value of \mathcal{B} can be placed by post-glitch relaxation data, using the two-fluid formalism (with the crust assumed rigidly attached to the ‘‘protons’’). For example, Vela’s 1988 ‘‘Christmas’’ glitch implies a crust-core coupling timescale $\tau_c \leq 300(I_1/I_s)$ s (Abney, Epstein & Olinto 1996). A simple glitch relaxation model can be constructed from eqns. (1)–(2), assuming rigid-body rotation for the fluids. The resulting coupling timescale due to mutual friction is found to be $\tau_{\text{mf}} = (I_1/I_s)/(2\Omega\mathcal{B})$, in agreement with the result of Andersson, Sidery & Comer (2006). For a rotation period $P = 2\pi/\Omega \sim 0.1$ s and $I_1 \approx 0.1I_s$, the requirement $\tau_{\text{mf}} < \tau_c$ provides the constraint $\mathcal{B} > 2 \times 10^{-5}$. This translates to either $\mathcal{R} > 2 \times 10^{-5}$ (weak drag) or $\mathcal{R} < 4 \times 10^4$ (strong drag).

Finally, it is worth making a few remarks on the precession model that we consider. Following Sedrakian, Wasserman & Cordes (1999) we assume that the global motion follows from (1) and (2) after imposing that each fluid rotates as a solid body. Misaligning the two rotation vectors we then arrive at a convenient two-component model for free precession which accounts for the damping due to mutual friction. The detailed precession modes are discussed in Appendix A. This model represents the current state-of-the-art in this problem area. However, it is obviously simplistic. The true ‘‘layering’’ of a real neutron star, and possible effects due to the various interfaces/boundaries are not accounted for. This means that one must be careful when trying to connect our model to detailed calculations for the various parameters, e.g. the mutual friction coefficients discussed by Andersson, Sidery & Comer (2006). Basically, the model should be seen as a *body averaged* representation of the real system, and the same is true for (say) the drag coefficient \mathcal{R} .

3 LOCAL WAVE ANALYSIS

The present investigation is motivated by the fact that a relative flow along a superfluid vortex array may trigger an instability that leads to the formation of vortex tangles and a state of superfluid turbulence, see Andersson, Sidery & Comer (2007); Sidery, Andersson & Comer (2007) for discussion and references to the relevant literature. Our aim is to find out whether this vortex instability may be active in a precessing neutron star.

As a first step we consider perturbations with respect to a stationary background configuration where both fluids rotate rigidly, i.e.

$$v_{\text{x}0}^i = \epsilon^{ijk} (\Omega_j^{\text{x}} - \Omega_{0j}) x_k, \quad \Omega_{\text{x}}^i = \text{constant} \quad (11)$$

allowing for an arbitrary orientation of the angular velocity vectors. After linearising and fixing $\Omega_0^i = \Omega_n^i = \Omega_n \hat{n}^i$, i.e.

² Neither will (5) result if the drag coefficient $\tilde{\mathcal{R}}$ is velocity dependent.

4 Glampedakis, Andersson & Jones

working in the neutron frame (for later convenience), the various quantities appearing in the Euler equations (1)-(2) become

$$v_{\mathbf{x}}^i \rightarrow v_{\mathbf{x}0}^i + v_{\mathbf{x}}^i, \quad v_{\mathbf{n}0}^i = 0, \quad v_{\mathbf{p}0}^i = \epsilon^{ijk}(\Omega_j^{\mathbf{p}} - \Omega_j^{\mathbf{n}})x_k$$

$$\omega_{\mathbf{n}}^i = 2\Omega_{\mathbf{n}}^i + \epsilon^{ijk}\nabla_j v_k^{\mathbf{n}}, \quad \hat{\omega}_{\mathbf{n}}^i = \hat{n}^i + \frac{1}{2\Omega_{\mathbf{n}}} \left(g^{ij} - \hat{n}^i \hat{n}^j \right) \delta\omega_j^{\mathbf{n}}$$

$$\psi_{\mathbf{x}} = \psi_{\mathbf{x}0} + \delta\psi_{\mathbf{x}}$$

We now focus our attention on short wavelength motion, such that we can analyse the dynamics without considering boundary conditions etcetera. In practice, we use the standard plane-wave decomposition

$$v_{\mathbf{x}}^i = A_{\mathbf{x}}^i e^{i\sigma t + ik_j x^j}, \quad A_{\mathbf{x}}^i = \text{constant} \quad (12)$$

in (1), (2) and (3). It is useful to decompose various vectors into a piece parallel to the vortex array and a piece that is orthogonal to it, i.e. use

$$A_{\mathbf{x}}^i = A_{\mathbf{x}}^{\parallel} \hat{n}^i + A_{\mathbf{x}}^{\perp, i} \quad (13)$$

and similarly for all other variables. Given that we have assumed that the fluids are incompressible, we must have

$$k_j A_{\mathbf{x}}^j = 0 \quad (14)$$

In other words, the waves we consider are transverse. To simplify the analysis somewhat, we will assume that the waves propagate along the vortex array in the following. This means that we align k^i with \hat{n}^i , see Sidery, Andersson & Comer (2007) for comments on this assumption. Hence we have

$$k_{\perp}^i = 0 \quad \Rightarrow \quad k^i = k_{\parallel} \hat{n}^i \quad (15)$$

and

$$\hat{n}_j A_{\mathbf{x}}^j = 0 \quad \Rightarrow \quad A_{\mathbf{x}}^{\parallel} = 0 \quad (16)$$

Finally, we define two additional unit vectors \hat{s}^i and $\hat{\lambda}^i$ to form an orthonormal triad,

$$\hat{s}^i \hat{n}_i = 0 \quad \text{and} \quad \hat{\lambda}^i = \epsilon^{ijk} \hat{s}_j \hat{n}_k \quad (17)$$

One of the key reasons why the above assumptions are useful is that we do not need to worry about the perturbations in the potentials $\psi_{\mathbf{x}}$. They are simply obtained by projecting the Euler equations onto \hat{n}^i . To determine a dispersion relation for the propagation and analyse the nature of the associated waves, it is sufficient to consider the equations obtained by projecting the Euler equations in the directions \hat{s}^i and $\hat{\lambda}^i$.

Finally, in order to write down the linearised version of the Euler equations (1) and (2) we need an expression for the perturbed mutual friction force. This can be written

$$\begin{aligned} \delta f_{\text{mf}}^i &= -2\Omega_{\mathbf{n}} \mathcal{B} (A_{\mathbf{n}}^i - A_{\mathbf{p}}^i) \\ &\quad + ik_{\parallel} \mathcal{B} \left(\hat{n}^i \epsilon_{jkl} w_0^j \hat{n}^k A_{\mathbf{n}}^l + w_{\parallel} \epsilon^{ijk} \hat{n}_j A_{\mathbf{k}}^n \right) \\ &\quad + 2\Omega_{\mathbf{n}} \mathcal{B}' \epsilon^{ijk} \hat{n}_j (v_k^{\mathbf{n}} - v_k^{\mathbf{p}}) + ik_{\parallel} \mathcal{B}' w_{0j} (\hat{n}^j A_{\mathbf{n}}^i - \hat{n}^i A_{\mathbf{n}}^j) \end{aligned} \quad (18)$$

3.1 Restricted problem: perturbations in neutron fluid only

Before considering the general solutions to the above equations it is useful to note that a simplified version of the present problem has already been discussed by Sidery, Andersson & Comer (2007) (see Glaberson, Johnson & Ostermeier (1974) for the analysis of the superfluid Helium case). They assume that the proton fluid is locked to its background value, $v_{\mathbf{p}0}^i = \epsilon^{ijk}(\Omega_j^{\mathbf{p}} - \Omega_j^{\mathbf{n}})x_k$ in our case, and that it is sufficient to consider only the neutron equation (1). It is useful to recall the results obtained for this simplified problem for two reasons. First of all, the discussion explains our general strategy. Secondly, and more importantly, we will later demonstrate that the results remain essentially unchanged in the weak drag limit.

Assuming that the protons remain unperturbed, we easily obtain

$$\begin{aligned} (i\sigma + 2\Omega_{\mathbf{n}} \mathcal{B} - i\mathcal{B}' k_{\parallel} w_{\parallel}) A_{\mathbf{n}}^i \\ + [(1 - \mathcal{B}') 2\Omega_{\mathbf{n}} - i\mathcal{B} k_{\parallel} w_{\parallel}] \epsilon^{ijk} \hat{n}_j A_{\mathbf{k}}^n = 0 \end{aligned} \quad (19)$$

where

$$w_{\parallel} = \hat{n}_i (v_{\mathbf{n}0}^i - v_{\mathbf{p}0}^i) = -\hat{n}_i v_{\mathbf{p}0}^i \quad (20)$$

Taking the inner product of (19) with $v_{\mathbf{n}}^i$ gives

$$(A_{\perp}^n)^2 = 0 \quad \Rightarrow \quad \hat{s}_i A_{\mathbf{n}}^i = \pm i (\hat{\lambda}_i A_{\mathbf{n}}^i) \quad (21)$$

Hence the modes under discussion represent circularly polarised waves. Next, projecting (19) along \hat{s}^i and $\hat{\lambda}^i$ we get

$$\begin{aligned} [2\mathcal{B}\Omega_{\mathbf{n}} + i(\sigma - \mathcal{B}' k_{\parallel} w_{\parallel})] (\hat{s}_i A_{\mathbf{n}}^i) \\ + [2(1 - \mathcal{B}')\Omega_{\mathbf{n}} - i\mathcal{B} w_{\parallel} k_{\parallel}] (\hat{\lambda}_i A_{\mathbf{n}}^i) = 0 \end{aligned} \quad (22)$$

$$\begin{aligned} [2(1 - \mathcal{B}')\Omega_{\mathbf{n}} - i\mathcal{B} w_{\parallel} k_{\parallel}] (\hat{s}_i A_{\mathbf{n}}^i) \\ - [2\mathcal{B}\Omega_{\mathbf{n}} + i(\sigma - \mathcal{B}' k_{\parallel} w_{\parallel})] (\hat{\lambda}_i A_{\mathbf{n}}^i) = 0 \end{aligned} \quad (23)$$

Requiring a non-trivial solution for this system we find the dispersion relation,

$$\sigma = [\mathcal{B}' k_{\parallel} w_{\parallel} \pm 2(1 - \mathcal{B}')\Omega_{\mathbf{n}}] + i\mathcal{B} (2\Omega_{\mathbf{n}} \mp k_{\parallel} w_{\parallel}) \quad (24)$$

Note that this result is valid for arbitrary \mathcal{B} and \mathcal{B}' , i.e. it is relevant for both the strong and weak drag limits. It is also in agreement with the result found by Glaberson, Johnson & Ostermeier (1974) in the limit of purely transverse waves, and Sidery, Andersson & Comer (2007) in the limit $\mathcal{B}' \rightarrow 0$.

In the limit of vanishing mutual friction the dispersion relation reduces to $\sigma = \pm 2\Omega_{\mathbf{n}}$. These modes represent collective vortex Kelvin oscillations. At the macroscopic level these waves can be identified with inertial waves in the neutron fluid (Sonin 1987; Sidery, Andersson & Comer 2007). In the presence of mutual friction the inertial modes are generally damped but, remarkably, they may become *unstable* when there is a relative flow along the vortex array. We have an instability when

$$\text{Im } \sigma < 0 \quad \Rightarrow \quad |w_{\parallel}| > \frac{2\Omega_{\mathbf{n}}}{k_{\parallel}} \quad (25)$$

In the case of superfluid Helium this instability was first discussed by Glaberson, Johnson & Ostermeier (1974), and

is often referred to as the Donnelly-Glaberson instability (Barenghi, Donnelly & Vinen 2001). In the context of neutron stars the instability was recently discussed by Sidery, Andersson & Comer (2007), who argued that is a typical “two-stream” instability, a generic property of multi-fluid systems (see Andersson, Comer & Prix (2004) for references to the relevant literature). The relevance of this instability for neutron stars has also been discussed by Peralta et al. (2005, 2006).

We want to consider these plane-wave results in the context of a neutron star that is freely precessing. This means that we need to connect the background that we have used in the plane-wave analysis to the global motion of a precessing star. In all current models of precession (see the discussion in Appendix A) it is assumed that the two components rotate as solid bodies. However, since the rotation axes are not aligned one would in general expect both Ω_n^i and Ω_p^i to be time dependent. Since they are taken to be constant in the plane-wave calculation it is obvious that the result is only valid on a timescale that is short compared to the variation in Ω_n^i and Ω_p^i . As we will argue later, the relevant timescale to compare to is the precession period. Hence our analysis is applicable only if the instability growth time is significantly shorter than the precession period.

It is also clear that the unstable waves need to have relatively short wavelength. This becomes obvious if we consider the explicit form for w_{\parallel} . For our problem we have

$$\begin{aligned} w_{\parallel} &= -\hat{n}_i v_{p0}^i = -\hat{n}^i \epsilon_{ijk} \Omega_p^j x^k \\ &= (\hat{\lambda}^i \Omega_p^i) (\hat{s}_j x^j) - (\hat{s}^i \Omega_p^i) (\hat{\lambda}_j x^j) \end{aligned} \quad (26)$$

This shows that the projection, w_{\parallel} , of the background flow along the direction of the neutron vortices varies with position. This obviously does not invalidate the plane-wave analysis, but it is clear that the characteristic lengthscale must be much smaller than the radius of the star.

Finally, we need to appreciate that there will also be a cut-off at short wavelengths. If we had accounted for the vortex tension in our analysis we would have found a slightly different instability criterion (Glaberson, Johnson & Ostermeier 1974; Sidery, Andersson & Comer 2007)

$$|w_{\parallel}| > \frac{2\Omega_n}{k_{\parallel}} + \nu k_{\parallel} \quad (27)$$

where ν represents the tension. From this it is clear that the tension tends to stabilise the system for large k_{\parallel} (short wavelengths). However, if we compare the relative magnitude of the terms in (27) we immediately see that the tension is rather insignificant. The two contributions are equal for a wavelength,

$$\begin{aligned} \nu k_{\parallel}^2 &= 2\Omega_n \quad \Rightarrow \\ \lambda_0 &= 2\pi \left(\frac{\nu}{2\Omega_n} \right)^{1/2} \approx 7 \times 10^{-2} \sqrt{P(s)} \text{ cm} \end{aligned} \quad (28)$$

where $P(s)$ is the rotation period in seconds. In other words, the tension contribution dominates only for wavelengths λ_0 comparable to the intervortex spacing

$$d_n \approx 10^{-2} \sqrt{P(s)} \text{ cm} \quad (29)$$

At that level the macroscopic hydrodynamics that we have

been using is no longer relevant. Equations (1)–(3) arrive after averaging over lengthscales much larger than d_n . Consequently, the plane wave analysis makes sense provided that $\lambda \gg d_n$, which also means that $\lambda \gg \lambda_0$. Hence, as far as the present hydrodynamics problem is concerned, we can always neglect the vortex tension. The vortex tension would be important if we were to consider the dynamics of a single vortex. In fact, an analysis of that problem shows that an oscillating vortex can also become unstable. The relevant instability criterion is similar to (27), although as expected for large k_{\parallel} the first term is irrelevant and the tension plays the key role.

3.2 Complete problem: perturbations in both fluids

In a neutron star core there is no compelling argument for clamping the proton fluid as we did in the previous example. It was a useful assumption because it simplified the algebra. It also provided a straightforward demonstration of the presence of unstable waves in the system. However, if we want to make contact with realistic precessing neutron star models we need a more detailed analysis. Hence, we consider the case where both fluids are perturbed.

In the general case we have the two equations of motion

$$\begin{aligned} (i\sigma + 2\Omega_n \mathcal{B} - i\mathcal{B}' w_{\parallel} k_{\parallel}) A_n^i & \\ - 2\Omega_n \mathcal{B} A_p^i + 2\Omega_n \mathcal{B}' \epsilon^{ijk} \hat{n}_j A_k^p & \\ + [2\Omega_n(1 - \mathcal{B}') - i\mathcal{B} w_{\parallel} k_{\parallel}] \epsilon^{ijk} \hat{n}_j A_k^n &= 0 \end{aligned} \quad (30)$$

and

$$\begin{aligned} \left[i\sigma + v_{ee} k_{\parallel}^2 - ik_{\parallel} w_{\parallel} + 2\Omega_n \left(\frac{\mathcal{B}}{x_p} \right) \right] A_p^i & \\ + \left[ik_{\parallel} w_{\parallel} \left(\frac{\mathcal{B}'}{x_p} \right) - 2\Omega_n \left(\frac{\mathcal{B}}{x_p} \right) \right] A_n^i & \\ + \left[ik_{\parallel} w_{\parallel} \left(\frac{\mathcal{B}}{x_p} \right) + 2\Omega_n \left(\frac{\mathcal{B}'}{x_p} \right) \right] \epsilon^{ijk} \hat{n}_j A_k^n & \\ + \left[\Omega_n \left(1 - \frac{2\mathcal{B}'}{x_p} \right) + \Omega_p^{\parallel} \right] \epsilon^{ijk} \hat{n}_j A_k^p &= 0 \end{aligned} \quad (31)$$

where $\Omega_p^{\parallel} = \hat{n}_i \Omega_p^i$. Projection of these equations along the \hat{s}^i and $\hat{\lambda}^i$ vectors results in the 4×4 system

$$\begin{aligned} (i\sigma + 2\mathcal{B}\Omega_n - i\mathcal{B}' w_{\parallel} k_{\parallel}) (\hat{s}_i A_n^i) - 2\Omega_n \mathcal{B} (\hat{s}_i A_p^i) & \\ + [2\Omega_n(1 - \mathcal{B}') - i\mathcal{B} w_{\parallel} k_{\parallel}] (\hat{\lambda}_i A_n^i) + 2\Omega_n \mathcal{B}' (\hat{\lambda}_i A_p^i) &= 0 \end{aligned} \quad (32)$$

$$\begin{aligned} (i\sigma + 2\mathcal{B}\Omega_n - i\mathcal{B}' w_{\parallel} k_{\parallel}) (\hat{\lambda}_i A_n^i) - 2\Omega_n \mathcal{B}' (\hat{\lambda}_i A_p^i) & \\ - [2\Omega_n(1 - \mathcal{B}') - i\mathcal{B} w_{\parallel} k_{\parallel}] (\hat{s}_i A_n^i) - 2\Omega_n \mathcal{B}' (\hat{s}_i A_p^i) &= 0 \end{aligned} \quad (33)$$

$$\begin{aligned} \left[i\sigma + v_{ee} k_{\parallel}^2 + 2\Omega_n \left(\frac{\mathcal{B}}{x_p} \right) - ik_{\parallel} w_{\parallel} \right] (\hat{s}_i A_p^i) & \\ + \left[ik_{\parallel} w_{\parallel} \left(\frac{\mathcal{B}'}{x_p} \right) - 2\Omega_n \left(\frac{\mathcal{B}}{x_p} \right) \right] (\hat{s}_i A_n^i) & \\ + \left[2\Omega_n \left(\frac{\mathcal{B}'}{x_p} \right) + ik_{\parallel} w_{\parallel} \left(\frac{\mathcal{B}}{x_p} \right) \right] (\hat{\lambda}_i A_n^i) & \\ + \left[\Omega_n \left(1 - 2\frac{\mathcal{B}'}{x_p} \right) + \Omega_p^{\parallel} \right] (\hat{\lambda}_i A_p^i) &= 0 \end{aligned} \quad (34)$$

$$\begin{aligned}
& \left[i\sigma + \nu_{ee}k_{\parallel}^2 + 2\Omega_n \left(\frac{\mathcal{B}}{x_p} \right) - ik_{\parallel}w_{\parallel} \right] (\hat{\lambda}_i A_p^i) \\
& + \left[ik_{\parallel}w_{\parallel} \left(\frac{\mathcal{B}'}{x_p} \right) - 2\Omega_n \left(\frac{\mathcal{B}}{x_p} \right) \right] (\hat{\lambda}_i A_n^i) \\
& - \left[2\Omega_n \left(\frac{\mathcal{B}'}{x_p} \right) + ik_{\parallel}w_{\parallel} \left(\frac{\mathcal{B}}{x_p} \right) \right] (\hat{s}_i A_n^i) \\
& - \left[\Omega_n \left(1 - 2\frac{\mathcal{B}'}{x_p} \right) + \Omega_p^{\parallel} \right] (\hat{s}_i A_p^i) = 0 \quad (35)
\end{aligned}$$

The dispersion relation associated with this system is a fourth order polynomial in σ . The roots can be explicitly calculated, but the dependence on the various parameters will be complicated. In order to explore the nature of the waves in the system it makes sense to focus on specific limiting cases. This way we also obtain useful approximate expressions for the growth time of the unstable modes. As a first approximation it is natural to consider the *inviscid* problem, i.e. we set $\nu_{ee} = 0$.

3.2.1 Approximate inviscid solutions

With the shear viscosity eliminated, we can arrive at different approximate solutions by considering, separately, (i) the short wavelength limit $k_{\parallel}R \rightarrow \infty$ and (ii) the weak/strong drag limits, $\mathcal{R} \rightarrow 0$ and $\mathcal{R} \rightarrow \infty$, respectively.

The short wavelength approximation leads to the following mode solutions, valid for every \mathcal{R} ,

$$\sigma_{1,2} \approx \pm 2\Omega_n + (i\mathcal{B} \mp \mathcal{B}') (2\Omega_n \mp k_{\parallel}w_{\parallel}) \quad (36)$$

$$\sigma_{3,4} \approx \pm(\Omega_n + \Omega_p^{\parallel}) + k_{\parallel}w_{\parallel} + \frac{2\Omega_n}{x_p}(i\mathcal{B} \mp \mathcal{B}') \quad (37)$$

The top pair is identical to the modes found in the problem where the protons were kept clamped. These modes can still become unstable under the action of mutual friction, and the instability criterion (25) remains *unchanged*.

For a generic value of \mathcal{R} both mode pairs in (36)-(37) describe waves where the neutron and proton fluids oscillate in concert. However, a closer look reveals their distinct nature. In the weak drag limit, $\mathcal{R} \rightarrow 0$, equations (30) and (31) decouple, and the modes (36) represent *pure* neutron fluid inertial waves, circularly polarised. The second pair of modes (37) are different, representing the proton inertial modes as viewed in a frame rotating with the neutrons. These modes are always damped by mutual friction.

Next, we derive approximate solutions for weak and strong drag without any limitation on the wavelength. The $\mathcal{R} \rightarrow 0$ case is the easiest. Retaining only the leading order mutual friction, the modes have the form (36)-(37) with $\mathcal{B}' = 0$. As we have just discussed, these are neutron inertial waves weakly coupled to the protons and vice-versa.

The strong coupling solutions are obtained after letting $\mathcal{B}' \rightarrow 1$ and $\mathcal{B} \rightarrow 0$ in the dispersion relation. Keeping the same identification for the modes as in (36)-(37), we find

$$\begin{aligned}
\sigma_{1,2} \approx & \pm \frac{1}{2} \left[\Omega_p^{\parallel} + \left(1 - \frac{2}{x_p} \right) \Omega_n \right] - k_{\parallel}w_{\parallel} \\
& - \frac{1}{2x_p} \left\{ (\Omega_p^{\parallel} + \Omega_n)^2 x_p^2 + 4\Omega_n [(1 + 3x_p)\Omega_n - x_p\Omega_p^{\parallel}] \right. \\
& \left. \mp 8x_p\Omega_n k_{\parallel}w_{\parallel} \right\}^{1/2} \quad (38)
\end{aligned}$$

$$\begin{aligned}
\sigma_{3,4} \approx & \pm \frac{1}{2} \left[\Omega_p^{\parallel} + \left(1 - \frac{2}{x_p} \right) \Omega_n \right] - k_{\parallel}w_{\parallel} \\
& + \frac{1}{2x_p} \left\{ (\Omega_p^{\parallel} + \Omega_n)^2 x_p^2 + 4\Omega_n [(1 + 3x_p)\Omega_n - x_p\Omega_p^{\parallel}] \right. \\
& \left. \mp 8x_p\Omega_n k_{\parallel}w_{\parallel} \right\}^{1/2} \quad (39)
\end{aligned}$$

It is clear that the strong drag coupling alters the waves in the system significantly. It is no longer the case that the neutrons and protons can oscillate “independently”. Moreover, the above results show that the system may now be unstable already at leading order (i.e. when $\mathcal{B}' = 1$ and $\mathcal{B} = 0$). In order to discuss this strong drag instability further we assume that Ω_p^i and Ω_n^i are almost aligned. As we will see later, this assumption is valid for the free precession motion. Setting $\Omega_p^{\parallel} \approx \Omega_n$ the mode-frequencies become

$$\begin{aligned}
\sigma_{1,2} \approx & \pm \Omega_n \left(1 - \frac{1}{x_p} \right) - k_{\parallel}w_{\parallel} \\
& - \frac{1}{x_p} \left[\Omega_n^2 (1 + x_p)^2 \mp 2\Omega_n k_{\parallel}w_{\parallel} x_p \right]^{1/2} \quad (40)
\end{aligned}$$

$$\begin{aligned}
\sigma_{3,4} \approx & \pm \Omega_n \left(\frac{1}{x_p} - 1 \right) - k_{\parallel}w_{\parallel} \\
& + \frac{1}{x_p} \left[\Omega_n^2 (1 + x_p)^2 \mp 2\Omega_n k_{\parallel}w_{\parallel} x_p \right]^{1/2} \quad (41)
\end{aligned}$$

From these results we see that the waves are unstable if

$$|w_{\parallel}| > \frac{\Omega_n(1 + x_p)^2}{2k_{\parallel}x_p} \quad (42)$$

This criterion is clearly different from the weak drag result, (25). Since x_p is expected to be small, the critical relative flow needs to be larger to trigger an instability in the strong drag case. However, the unstable modes no longer depend on the mutual friction coefficient \mathcal{B} , as they did in the weak drag case. Instead, the key coupling that facilitates the instability is due to $\mathcal{B}' \approx 1$.

It is relevant to make an observation at this point. While the weak drag instability is well known from studies of superfluid Helium, see Glaberson, Johnson & Ostermeier (1974); Sidery, Andersson & Comer (2007) for discussions, we believe that our work provides the first suggestion that an analogous instability may operate in the strong drag problem. Hence, the above results are exciting. Having said that, we can no longer rely on the analogy with the Helium case. In the weak drag situation there is a natural link between the instability and the transition to superfluid turbulence (Andersson, Sidery & Comer 2007). In the strong drag case, it may seem natural to expect that the unstable modes still lead to the formation of vortex tangles. However, given the stronger coupling between the two fluids in the system the problem is different, and will require further analysis in order to be understood.

3.2.2 Adding shear viscosity

The previous results were derived assuming vanishing shear viscosity, for the purpose of understanding the properties of the various types of inertial waves. However, viscosity could play an important role in the problem due to the small scales involved. At the end of the day, if an instability is triggered

in the inertial waves shear viscosity should be the main counteracting agent and in order to arrive at realistic estimates for the growth time of the instability we need to account for it. Having said that, it is important to bear in mind that the various inertial waves will be affected by viscosity in drastically different ways. The key point is that only the proton fluid is directly coupled to the mechanism that generates viscosity (recall that protons, electrons and the magnetic fluxtubes are all assumed to be “locked” together) while any communication with the neutron component is mediated by the mutual friction. This feature is clearly encoded in the hydrodynamical equations (1)-(2).

The interplay between mutual friction and viscous coupling is exposed if we amend the approximate mode solutions from the preceding Section with viscosity. Considering first the short wavelength limit we now find

$$\begin{aligned} \sigma_{1,2} \approx \pm 2\Omega_n + (i\mathcal{B} \mp \mathcal{B}')(2\Omega_n \mp k_{\parallel} w_{\parallel}) \\ \pm \frac{2i\Omega_n w_{\parallel}}{\nu_{ee} k_{\parallel} x_p} [\mathcal{B}^2 - (\mathcal{B}')^2] \end{aligned} \quad (43)$$

$$\begin{aligned} \sigma_{3,4} \approx \pm(\Omega_n + \Omega_p^{\parallel}) + k_{\parallel} w_{\parallel} \\ + \frac{2\Omega_n}{x_p} (i\mathcal{B} \mp \mathcal{B}') + i\nu_{ee} k_{\parallel}^2 \end{aligned} \quad (44)$$

where in each case we have kept only the leading order viscous term³. The key result is that only the “proton” modes $\sigma_{3,4}$ are damped by viscosity in the usual way, that is, via a $i\nu_{ee} k_{\parallel}^2$ term which dominates at small scales. In contrast, the viscosity dependence of the “neutron” modes $\sigma_{1,2}$ is intimately linked to the mutual friction coupling, leading to a perhaps surprising scaling with negative powers of k_{\parallel} .

As in the inviscid problem, the $\mathcal{R} \rightarrow 0$ solutions simply follow from (43) and (44) after setting $\mathcal{B} = \mathcal{B}' = 0$. In this limit the $\sigma_{1,2}$ modes are essentially not affected by viscosity. This is not surprising since they describe oscillations in the neutron fluid only.

In the strong drag limit we find the following viscous modes (assuming $\Omega_p^{\parallel} \approx \Omega_n$), which generalise (40) and (41),

$$\begin{aligned} \sigma_{1,2} \approx \pm \Omega_n \left(1 - \frac{1}{x_p} \right) + k_{\parallel} w_{\parallel} + \frac{i}{2} \nu_{ee} k_{\parallel}^2 \\ - \frac{1}{x_p} \left[-\frac{1}{4} (\nu_{ee} k_{\parallel}^2 x_p)^2 \pm i x_p (x_p - 1) \Omega_n \nu_{ee} k_{\parallel}^2 \right. \\ \left. + \Omega_n^2 (1 + x_p)^2 \mp 2\Omega_n k_{\parallel} w_{\parallel} x_p \right]^{1/2} \end{aligned} \quad (45)$$

$$\begin{aligned} \sigma_{3,4} \approx \pm \Omega_n \left(1 - \frac{1}{x_p} \right) + k_{\parallel} w_{\parallel} + \frac{i}{2} \nu_{ee} k_{\parallel}^2 \\ + \frac{1}{x_p} \left[-\frac{1}{4} (\nu_{ee} k_{\parallel}^2 x_p)^2 \pm i x_p (x_p - 1) \Omega_n \nu_{ee} k_{\parallel}^2 \right. \\ \left. + \Omega_n^2 (1 + x_p)^2 \mp 2\Omega_n k_{\parallel} w_{\parallel} x_p \right]^{1/2} \end{aligned} \quad (46)$$

Not surprisingly these expressions admit an instability at leading order (top pair), but they also demonstrate the contrasting viscosity dependence. To see this, consider the first

pair of solutions and assume that the viscosity is negligible. Then increase $\nu_{ee} k_{\parallel}^2$ while keeping all other parameters fixed. It is then easy to see that, once the leading viscous term under the square-root becomes dominant, there will be a cancellation with the other $i\nu_{ee} k_{\parallel}^2/2$ term. Thus, the leading viscous damping term does not have the expected form, it is much weaker. This is in contrast to the result for the second pair of solutions. In that case the two viscosity terms combine to give the anticipated $i\nu_{ee} k_{\parallel}^2$ damping term.

All these approximate viscous solutions convey the same physical information. The modes that represent pure neutron inertial waves in the limit of vanishing mutual friction exhibit an unconventional – and much weaker – dependence on shear viscosity. These are also the *only* modes that can become unstable and lead to the formation of vortex tangles and turbulence.

3.3 Growth timescales

The numerical solution of the full system (32)-(35) unveils the presence of an instability for a large portion of the parameter space and, as we show below, the associated growth time $\tau_{\text{grow}} = 1/\text{Im } \sigma$ can be quite short. The numerical timescales can be well approximated by the preceding analytic mode solutions (for different wavelength ranges). Hence, we are able to provide simple analytic estimates for τ_{grow} . These estimates will be a useful tool in our discussion of precessing neutron stars.

The first estimate follows from the short wavelength results, (36) or (43),

$$\tau_{\text{grow}} \approx \frac{1}{2\Omega_n \mathcal{B}} \left(\frac{\pi |w_{\parallel}|}{\Omega_n \lambda} - 1 \right)^{-1} \quad (47)$$

Based on our previous discussion we expect this result to be accurate also in the weak drag limit, irrespective of wavelength (provided of course that $\lambda \ll R$).

A second estimate is relevant in the strong coupling regime. Since the relevant mode solutions are sensitive to viscosity, we need to distinguish between the inviscid and the viscous case. For the former we find from (40),

$$\tau_{\text{grow}} \approx \frac{x_p(1-x_p)}{\Omega_n} \left(\frac{4\pi |w_{\parallel}| x_p}{\Omega_n \lambda} - 1 \right)^{-1/2} \quad (48)$$

In the viscous case it is not easy to extract a similarly simple estimate. This is not surprising since the modes (45) are more complicated than the inviscid ones. Hence, we calculate $1/\text{Im } \sigma$ numerically in this case.

Our results for the instability growth times are illustrated in Figures 1-5. In the figures we compare the different approximations for τ_{grow} to the full numerical results. The data in the figures are obtained using a w_{\parallel} corresponding to a mismatch between Ω_p^i and Ω_n^i of 1° and a rotation period of 1 s. Later we will relate these results to actual precession solutions.

Let us first consider Figure 1, where we show the growth time as a function of the wavelength for fixed temperature and drag coefficient. The data concerns the intermediate and weak drag regimes, explicitly $\mathcal{R} = 1$ and $\mathcal{R} = 10^{-3}$. As we discussed earlier, there will be a short wavelength cut-off. A more detailed analysis would link this to the validity of the averaging that led to the macroscopic hydrodynamics

³ It is worth noting that these results are obtained by holding ν_{ee} fixed and then taking the large k_{\parallel} limit. In effect, this means that one cannot use these expressions to deduce the $\nu_{ee} \rightarrow 0$ behaviour.

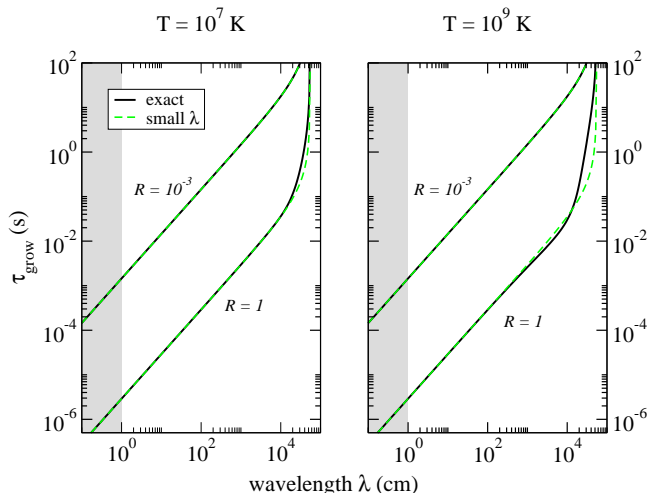


Figure 1. Numerical results (solid lines) for the instability growth time τ_{grow} as a function of the wavelength λ , for two choices for the core temperature, $T = 10^7$ K and 10^9 K (left and right panel, respectively). The analytic short wavelength approximation discussed in the main text is superimposed (dashed lines). The results represent weak ($\mathcal{R} = 10^{-3}$) and intermediate ($\mathcal{R} = 1$) drag. The angle between $\vec{\Omega}_n$ and $\vec{\Omega}_p$ is taken to be 1° and the rotational period is $P = 1$ s. The short-wavelength cut-off, which is about 1 cm for this rotation rate, is indicated by a grey area.

equations (1) and (2). This is a very difficult problem. To make immediate progress, we will simply assume that the instability analysis becomes invalid once the wavelength is so short that the fluid description is no longer valid. Then it seems reasonable to use something like

$$\lambda_{\text{min}} \approx 100d_n \approx \left(\frac{P}{1\text{s}}\right)^{1/2} \text{ cm} \quad (49)$$

The expected short-wavelength cut-off for a rotation period $P = 1$ s is then about 1 cm, as indicated in the figure. From these results it is clear that the short wavelength approximation (47) is very good for (essentially) the entire λ range and all relevant temperatures.

In the strong drag regime, for $\mathcal{R} \gg 1$, the variation of growth time with wavelength is more complicated, cf. Figure 2 which shows data for $\mathcal{R} = 10^3$. The small λ approximation again matches the exact result well in the region near the short wavelength cut-off, but it is not accurate for all wavelengths. For intermediate wavelengths the strong drag viscous solution (45) is more suitable. By combining the two approximations we arrive at an almost perfect agreement with the numerical results, including the transition region where shear viscosity is relevant. It is also apparent from the figure that the inviscid estimate (48) is accurate only for relatively hot stars, for which shear viscosity is weak. This is as expected.

We get a different view of the results if we fix the wavelength and vary the drag coefficient \mathcal{R} . Figure 3 shows such results for a rotation period of $P = 1$ s at the corresponding short wavelength cut-off, i.e. $\lambda = 1$ cm. From the left panel we see that the small λ approximation (47) is accurate for $\mathcal{R} < 10^7$ or so at $T = 10^7$ K. The remaining parameter space is well approximated by the viscous $\mathcal{R} \rightarrow \infty$ solution (43). The inviscid strong-drag approximation (48) is never really adequate for this very short wavelength. Simi-

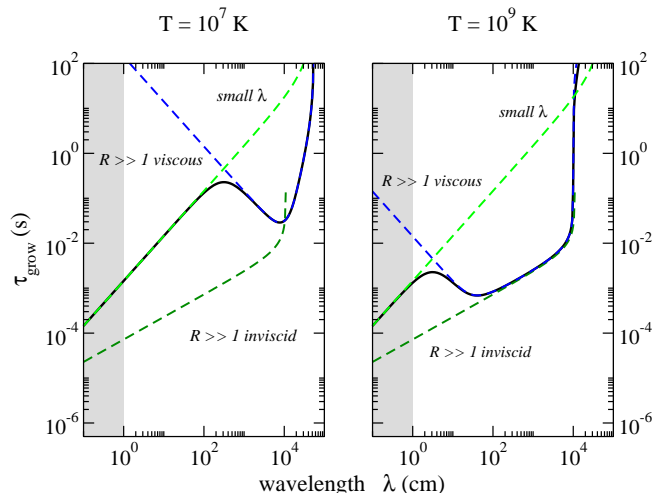


Figure 2. Same as Figure 1, but for strong drag $\mathcal{R} = 10^3$. In this regime, shear viscosity affects the results for intermediate wavelengths (around $\lambda = 1000$ cm and 10 cm in the left and right panels, respectively.) The various approximations discussed in the main text are superimposed (dashed lines). It is important to note that the unstable modes are not strongly affected by shear viscosity in the short wavelength limit.

lar results for $\lambda = 100$ cm are shown in Figure 4. Note that in both figures the growth time is shortest for \mathcal{R} of order unity, and the general behaviour follows immediately from $\tau_{\text{grow}} \sim 1/\mathcal{B} \sim \mathcal{R} + 1/\mathcal{R}$. This is analogous to the fact that the glitch relaxation timescale is expected to be long in both the weak and the strong drag limit (Alpar & Sauls 1988).

One can show that for very strong coupling, $\mathcal{R} > 10^5$ or so, the fastest growing waves are those with moderately short wavelengths, $\lambda > 100$ cm. For such large values of \mathcal{R} the mode solution (45) is accurate even for very short wavelengths. Whether this very strong drag regime is physically relevant is not clear.

From these comparisons with the numerical results we arrive at a practical guide to the validity of the analytic timescale estimates. For a wide range of \mathcal{R} the fastest growing modes are in the short wavelength regime near the cut-off, i.e. $\lambda \sim 1$ cm for $P = 1$ s, where the estimate (47) applies. For very strong coupling (depending on the temperature) the instability grows faster in modes with moderately short wavelengths (above $\lambda \sim 100$ cm) in which case (45) applies. In fact, this approximation tends to be good for intermediate wavelengths at all temperatures for strong drag.

4 ARE PRECESSING NEUTRON STARS STABLE?

In order to address this key question we first need to discuss the “standard” two-fluid model for neutron star precession (Sedrakian, Wasserman & Cordes 1999) in some detail. A self-contained discussion of the relevant precession modes can be found in Appendix A. We want to combine these precession solutions with the preceding plane-wave analysis to establish whether the superfluid instability is present or not. In principle, this analysis may provide us with a “no-go

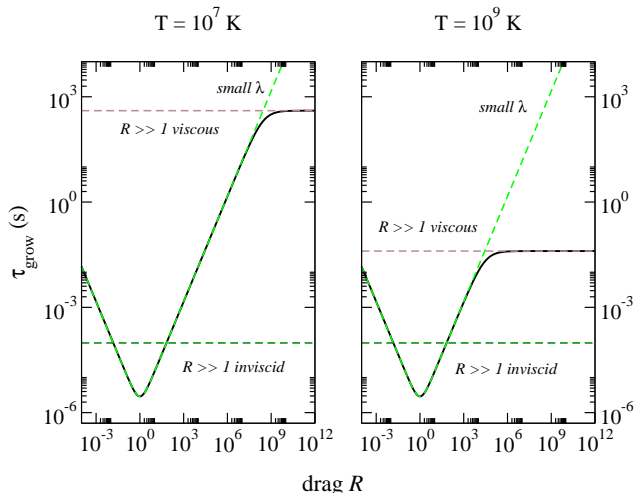


Figure 3. Numerical results (solid lines) for the instability growth time τ_{grow} as a function of mutual friction drag \mathcal{R} for two choices of core temperature, $T = 10^7$ K and 10^9 K (left and right panel, respectively). The analytic approximations discussed in the main text are superimposed (dashed lines). Here we have taken the wavelength to be that of the short wavelength cut-off, i.e. for $P = 1$ s we have $\lambda = 1$ cm. The angle between $\hat{\Omega}_n$ and $\hat{\Omega}_p$ is assumed to be 1°

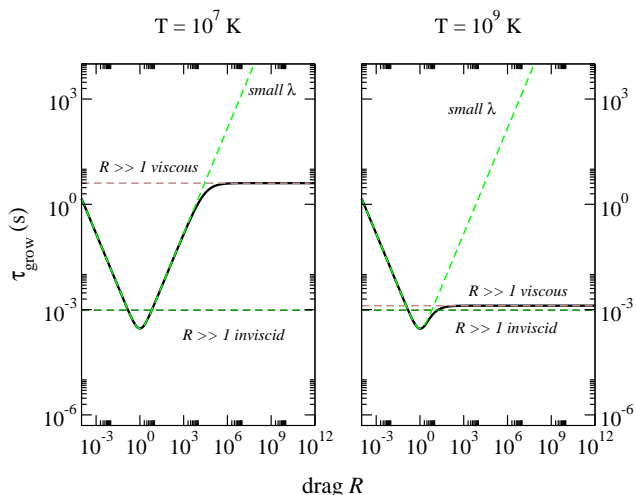


Figure 4. Same as Figure 3, but for $\lambda = 100$ cm.

theorem” for neutron star precession. After all, the precession modes are obtained by assuming global solid body rotation. If the corresponding solution exhibits a rapidly growing short wavelength instability, then the assumption of solid body rotation does not hold. The precession solution would simply be inconsistent. The upshot of this would be that one cannot neglect the hydrodynamical degrees of freedom of the precession problem. Any analysis of the precession problem would have to account for the hydrodynamics of the neutron star core, which would be a serious computational challenge.

In our analysis of the precession modes in Appendix A we go beyond the original work of Sedrakian, Wasserman & Cordes (1999) by providing general expressions for the precession period P_{pr} , the damping time τ_d and the angular amplitude θ_w (the so-called

“wobble” angle) for arbitrary mutual friction coupling. These are the key parameters⁴ which enable us to make contact with the two-fluid instability analysis. However, it turns out that the range of \mathcal{R} for which precession is not overdamped by mutual friction (in the sense that $\tau_d > P_{\text{pr}}$) is entirely covered by the approximate (weak and strong drag) results of Sedrakian, Wasserman & Cordes (1999). This is clearly illustrated in Figure A1. Therefore we only discuss results for the stability of precession in the limits of weak and strong drag.

From the practical point of view, the perturbative calculation in Section 3 assumes a static background. Therefore a given precession mode can only serve as background provided that the unstable waves grow fast enough. To ensure that this is the case, we will require $\tau_{\text{grow}} \ll \min(P_{\text{pr}}, \tau_d)$ for the instability to be astrophysically relevant in a precessing star.

4.1 Weak drag precession

As described in Appendix A, there are two precession modes for any given value of the mutual friction parameter \mathcal{R} . Let us first consider the case of weak drag precession ($\mathcal{R} \ll 1$) and the mode that, in this weak coupling limit, reduces to the standard classical free precession of a biaxial body (i.e. to the sort of precession commonly considered in the literature, see e.g. Jones & Andersson (2001); Link & Epstein (2001)). This mode represents weakly damped, long-period precession with

$$P_{\text{pr}} = \frac{P}{\epsilon} \quad (50)$$

where ϵ is the (dimensionless) deformation associated with the biaxiality in the crust’s moment of inertia (see Appendix A). For PSR B1828-11 this deformation is estimated to be $\epsilon \approx 10^{-8}$. Moreover, assuming that PSR B1828-11 is described by the weak drag precession solution, one should be able to constrain \mathcal{B} using the fact that since its discovery (Stairs, Lyne & Shemar 2000) several undamped precession oscillations have been monitored. If N is the number of oscillations then we should have $\tau_d > NP_{\text{pr}}$ from which we find $\mathcal{R} < (0.16/N)(I_1/I_s)$. Using $N \approx 10$ and $I_1/I_s \approx 0.1$ we find $\mathcal{R} < 2 \times 10^{-3}$. Combining this upper limit with the lower limit placed by Vela’s glitch relaxation timescale we find that only a relatively narrow interval of weak drag mutual friction is allowed, $2 \times 10^{-5} < \mathcal{R} < 2 \times 10^{-3}$. Interestingly, the value suggested by Alpar, Langer & Sauls (1984); Andersson, Sidery & Comer (2006), $\mathcal{R} \sim 10^{-4}$, falls within this range.

The weak drag instability criterion (25) implies that waves with wavelength shorter than

$$\lambda_{\text{max}} = \frac{\pi|w_{\parallel}|}{\Omega_n} \quad (51)$$

are unstable. For the given weak drag precession solution we have (Appendix A)

$$w_{\parallel} \leq \epsilon \theta_w \Omega R \quad (52)$$

⁴ Note that P_{pr} and θ_w are in fact observable quantities, extracted from the timing data of the candidate precessors (Jones & Andersson 2001; Link & Epstein 2001).

which means that

$$\begin{aligned} \lambda_{\max} &\leq \pi \epsilon \theta_w R \\ &\approx 5.4 \times 10^{-4} \left(\frac{\theta_w}{1^\circ} \right) \left(\frac{\epsilon}{10^{-8}} \right) \left(\frac{R}{10^6 \text{ cm}} \right) \text{ cm} \end{aligned} \quad (53)$$

Since we need to have $\lambda_{\max} > \lambda_{\min}$ in order to argue that the instability is relevant we see that we must have

$$\left(\frac{\theta_w}{1^\circ} \right) > 1900 \left(\frac{P}{1 \text{ s}} \right)^{1/2} \left(\frac{\epsilon}{10^{-8}} \right)^{-1} \left(\frac{R}{10^6 \text{ cm}} \right)^{-1} \quad (54)$$

In words, this inequality gives the wobble angle required for the fluid in at least some portion of the star to be unstable for inertial waves with $\lambda = \lambda_{\min}$.

To demonstrate that the instability analysis is consistent we need to show that the growth time for the unstable modes is short compared to the precession period. Using (47), which according to Figure 1 matches the exact weak drag numerical results, we find

$$\tau_{\text{grow}} \approx \frac{\lambda}{2\pi \mathcal{B} |w_{\parallel}|} \quad (55)$$

This should be a good approximation for the shortest wavelength modes in the problem. Using the relevant result (52) for w_{\parallel} we find that

$$\begin{aligned} \tau_{\text{grow}} &> \\ 4 \times 10^{11} \left(\frac{\mathcal{B}}{4 \times 10^{-4}} \right)^{-1} \left(\frac{\epsilon}{10^{-8}} \right)^{-1} \left(\frac{\theta_w}{1^\circ} \right)^{-1} \left(\frac{P}{1 \text{ s}} \right) \left(\frac{\lambda}{R} \right) \text{ s} \end{aligned} \quad (56)$$

On the other hand, the precession period is

$$P_{\text{pr}} \approx 10^8 \left(\frac{\epsilon}{10^{-8}} \right)^{-1} \left(\frac{P}{1 \text{ s}} \right) \text{ s} \quad (57)$$

Requiring that $\tau_{\text{grow}} < 0.1 P_{\text{pr}}$ we see that we must have

$$\lambda < 25 \left(\frac{\mathcal{B}}{4 \times 10^{-4}} \right) \left(\frac{\theta_w}{1^\circ} \right) \left(\frac{R}{10^6 \text{ cm}} \right) \text{ cm} \quad (58)$$

We need to ask whether there is room for unstable waves with wavelengths longer than λ_{\min} . This would be the case if

$$\left(\frac{\theta_w}{1^\circ} \right) > 4 \times 10^{-2} \left(\frac{\mathcal{B}}{4 \times 10^{-4}} \right)^{-1} \left(\frac{R}{10^6 \text{ cm}} \right)^{-1} \left(\frac{P}{1 \text{ s}} \right)^{1/2} \quad (59)$$

In words, this inequality gives the wobble angle required for the unstable $\lambda = \lambda_{\min}$ inertial waves in some portion of the star to have a growth time of less than a tenth of the free precession period. Compared to (54) this restriction on the wobble angle is clearly much less stringent. Hence, we learn that whenever the instability is active the growth time τ_{grow} is much shorter than the precession period.

If we associate the instability with the onset of superfluid turbulence (see Andersson, Sidery & Comer (2007)) then only stars that satisfy the criterion (54) are likely to be turbulent. Note that this hardly constrains the realistic parameter space since according to the data all candidate precessors have $\epsilon \sim 10^{-7} - 10^{-8}$. Hence it would seem safe to conclude that this instability does not play a role in systems where the drag is weak, unless they are significantly deformed. However this does not mean that the instability criterion (54) is not astrophysically relevant. For example, a

millisecond pulsar with (say) $P = 1.5$ ms and $\epsilon = 5 \times 10^{-7}$ (which is a realistic value) would undergo an instability for a wobble angle $\theta_w > 1.5^\circ$. A more extreme example would be the suggested sighting of free precession of the SN1987A remnant (Middleditch et al. 2000a,b). Taking a spin period of 2.14 ms and a free precession period of $\sim 10^3$ s, we would have $\epsilon \approx 2 \times 10^{-6}$. For these values, the instability criterion (54) would be satisfied for $\theta_w > 0.4^\circ$. As discussed by Jones & Andersson (2001), the wobble angle would have to be much larger than 1° in order to explain the observations. In other words, this system would suffer the superfluid instability.

Now consider the second mode in the weak coupling limit. As discussed in Appendix A, in the case of zero coupling this mode simply corresponds to a misalignment between the rotation axes of the neutron and proton fluids, with both angular velocity vectors fixed in the inertial frame, i.e. no precession. Weak coupling then serves to induce a slow precession, with the star rotating about the 3-axis of the biaxial crust, and with this axis itself tracing out a cone at the longer free precession period. This is the opposite of the standard free precession motion of the first mode, where the 3-axis traces out a cone in space at the ‘‘spin’’ frequency, with a slow additional precession rotation superimposed.

However, from the observational point of view, both motions would produce modulations in the radio data and so this second mode cannot be discounted. A crucial difference is that for this second mode the ratio P_{pr}/P is determined not by the biaxiality of the crust ϵ , but instead by the strength of the coupling. We have

$$\frac{P}{P_{\text{pr}}} \approx \mathcal{R} \frac{I_1}{I_s + I_1} \quad (60)$$

The observed $P/P_{\text{pr}} \sim 10^{-8}$ would then give an estimate of $\mathcal{R} \sim 10^{-7}$ or less. This is smaller than the typical estimates based on microphysical considerations (see for example Andersson, Sidery & Comer (2006)) and is also smaller than the lower bound placed on \mathcal{R} from glitch observations (see discussion at the end of Section 2), arguing against this mode as an explanation of the PSR B1828-11 observations.

A further argument against this mode being relevant comes from our stability analysis. For this mode we find that

$$w_{\parallel} \leq \tilde{I} \theta_w \Omega R \quad (61)$$

and the instability is present for wavelengths shorter than

$$\lambda_{\max} = \pi \tilde{I} \theta_w R \quad (62)$$

where

$$\tilde{I} = 1 + \frac{I_1}{I_s} \quad (63)$$

This means that, if we require $\lambda_{\max} > \lambda_{\min}$ then an instability is present if

$$\left(\frac{\theta_w}{1^\circ} \right) > 2 \times 10^{-5} \frac{1}{\tilde{I}} \left(\frac{P}{1 \text{ s}} \right)^{1/2} \left(\frac{R}{10^6 \text{ cm}} \right)^{-1} \quad (64)$$

Alternatively, this can be expressed as a constraint on the rotation period. To avoid the instability we require

$$P > 3 \times 10^9 \tilde{I}^2 \left(\frac{\theta_w}{1^\circ} \right)^2 \left(\frac{R}{10^6 \text{ cm}} \right)^2 \text{ s} \quad (65)$$

As one would have expected given the large relative flow associated with it, this mode is seriously affected by the superfluid instability. The growth time is

$$\tau_{\text{grow}} > 3.6 \times 10^3 \frac{1}{\tilde{I}} \left(\frac{P}{1\text{s}} \right) \left(\frac{\mathcal{B}}{4 \times 10^{-4}} \right)^{-1} \left(\frac{\theta_w}{1^\circ} \right)^{-1} \left(\frac{\lambda}{R} \right) \text{ s} \quad (66)$$

If we require that this is smaller than a tenth of the precession period, then we must have

$$\lambda < 3 \times 10^2 \tilde{I} \left(\frac{\mathcal{B}}{4 \times 10^{-4}} \right) \left(\frac{\theta_w}{1^\circ} \right) \text{ cm} \quad (67)$$

Finally, requiring this to be larger than the cut-off λ_{min} we see that the instability is present for

$$\left(\frac{\theta_w}{1^\circ} \right) > 3 \times 10^{-3} \frac{1}{\tilde{I}} \left(\frac{\mathcal{B}}{4 \times 10^{-4}} \right)^{-1} \left(\frac{P}{1\text{s}} \right)^{1/2} \quad (68)$$

The analysis suggests that this mode would be unstable for any significant misalignment. It is therefore unlikely to be present in real stars.

4.2 Strong drag precession

For strong mutual friction the nature of the precessional motion changes significantly. To some extent, this was first discussed by Shaham (1977), see Appendix A for details. Precession is fast, with period

$$P_{\text{pr}} \approx P \left(\epsilon + \frac{1}{x_{\text{p}}} \right)^{-1} \approx x_{\text{p}} P \quad (69)$$

As we discussed in Section 3.3, in the case of strong drag the instability is sensitive to the action of viscosity and as a consequence the “window” of the fastest growing wavelengths shifts with varying \mathcal{R} . The most natural choice is to assume that $1 \ll \mathcal{R} < 10^5$ (see discussion at the end of Section 2) which means that the small λ approximation (47) for τ_{grow} describes the fastest growing waves accurately. We again have (55), which can be combined with the obtained approximation for w_{\parallel} (Appendix A)

$$w_{\parallel} \leq \frac{\theta_w \Omega R}{x_{\text{p}}} \quad (70)$$

For typical parameters we find

$$\tau_{\text{grow}} > 140 \left(\frac{x_{\text{p}}}{0.1} \right) \left(\frac{\theta_w}{1^\circ} \right)^{-1} \left(\frac{P}{1\text{s}} \right) \left(\frac{\mathcal{R}}{10^3} \right) \left(\frac{\lambda}{R} \right) \text{ s} \quad (71)$$

For consistency τ_{grow} needs to be shorter than the precession period (69). Requiring $\tau_{\text{grow}} < 0.1 P_{\text{pr}}$ as before, this restricts the wavelength to

$$\lambda < 70 \left(\frac{\mathcal{R}}{10^3} \right)^{-1} \left(\frac{\theta_w}{1^\circ} \right) \text{ cm} \quad (72)$$

The short lengthscale cut-off obviously remains as in the weak drag case. Thus we see that we need

$$\left(\frac{\theta_w}{1^\circ} \right) > 1.4 \times 10^{-2} \left(\frac{\mathcal{R}}{10^3} \right) \left(\frac{P}{1\text{s}} \right)^{1/2} \quad (73)$$

in order for the instability to be relevant. This clearly sets a very severe constraint on the fast precession solution.

The above results are, however, only relevant for short wavelengths. It is, of course, straightforward to find the general solution numerically. This provides the exact τ_{grow} as

shown in Figure 5. The numerical timescales corroborate the analytic estimates. For a large part of the parameter space the instability grows at sub-millisecond timescales, much faster than the precession period. This would be the case, for example, for PSR B1828-11 ($P \approx 0.4$ s, $T \sim 10^7$ K) if it were to precess under strong mutual friction.

As we have already discussed, the strong-drag results are temperature dependent. This is clear from the results shown in Figure 5. For very large \mathcal{R} , the fastest growing instability is no longer associated with the short-wavelength cut-off region. Instead, the fastest τ_{grow} is temperature dependent. This longer wavelength part of the instability window can be understood from (45) and (46). For longer wavelengths (small k_{\parallel}) one would expect shear viscosity to be unimportant. Thus the modes of the system should be well approximated by the inviscid result. In the inviscid case (45) implies that waves with wavelength shorter than

$$\lambda_{\text{max}} \approx \frac{4\pi |w_{\parallel}|}{\Omega_{\text{n}}} \frac{x_{\text{p}}}{(1+x_{\text{p}})^2} \approx \frac{4\pi x_{\text{p}} |w_{\parallel}|}{\Omega_{\text{n}}} \quad (74)$$

will be unstable. Working out the associated growth time we find

$$\tau_{\text{grow}} > 3.4 \times 10^{-2} \left(\frac{x_{\text{p}}}{0.1} \right) \left(\frac{\theta_w}{1^\circ} \right)^{-1/2} \left(\frac{P}{1\text{s}} \right) \left(\frac{\lambda}{R} \right)^{1/2} \text{ cm} \quad (75)$$

This estimate should be valid for long wavelengths ($< \lambda_{\text{max}}$) and/or high temperatures. As we move towards shorter wavelengths at fixed T , the importance of shear viscosity will increase, cf. Figure 5. To estimate the point at which the viscous contribution becomes important we can balance the first and last terms under the square-root in (45). That is, we consider

$$\frac{1}{4} \nu_{\text{ee}}^2 k_{\parallel}^4 x_{\text{p}}^2 = 2\Omega_{\text{n}} k_{\parallel} |w_{\parallel}| x_{\text{p}} \quad (76)$$

This suggests that the viscosity starts to play a role when

$$\lambda \approx 360 \left(\frac{P}{1\text{s}} \right)^{2/3} \left(\frac{R}{10\text{ km}} \right)^{-1/3} \left(\frac{\theta_w}{1^\circ} \right)^{-1/3} \left(\frac{x_{\text{p}}}{0.1} \right)^{2/3} \left(\frac{T}{10^8 \text{K}} \right)^{-4/3} \text{ s} \quad (77)$$

Combining this with the inviscid growth timescale (75) we find

$$\tau_{\text{grow}} \approx 6 \times 10^{-4} \left(\frac{P}{1\text{s}} \right)^{4/3} \left(\frac{\theta_w}{1^\circ} \right)^{-2/3} \left(\frac{x_{\text{p}}}{0.1} \right)^{4/3} \left(\frac{T}{10^8 \text{K}} \right)^{-2/3} \text{ s} \quad (78)$$

Adding the estimated $(\lambda, \tau_{\text{grow}})$ points to the data in Figure 5 we see that we have arrived at a reasonable approximation for the fastest growing mode in the intermediate wavelength regime. Finally, we can use this estimate to check when one would expect there to be such an instability window. If we require $\tau_{\text{grow}} < 0.1 P_{\text{pr}}$ as usual, then we find that the longer wavelength instability is present for

$$T > 1.5 \times 10^6 \left(\frac{P}{1\text{s}} \right)^{1/2} \left(\frac{\theta_w}{1^\circ} \right)^{-1} \left(\frac{x_{\text{p}}}{0.1} \right)^{1/2} \text{ K} \quad (79)$$

To conclude, our results provide a strong indication that the fast precession solution may not be relevant for realistic systems. Since it is generically unstable to small scale inertial waves the solid-body rotation assumption does not hold and the solution is inconsistent.

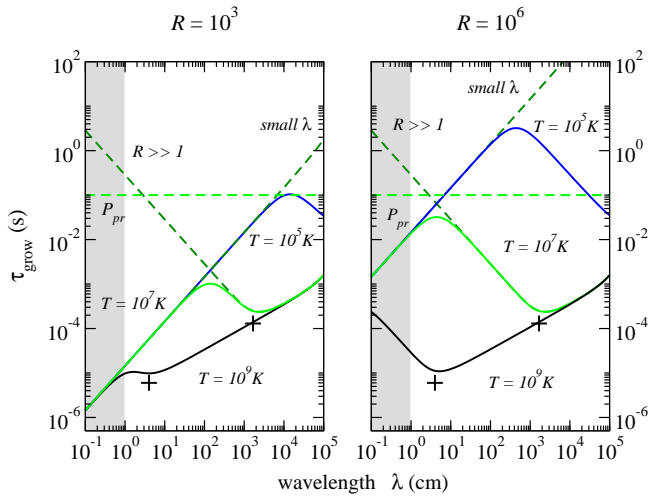


Figure 5. Instability growth times $\tau_{\text{grow}}(\lambda)$ for strong drag fast precession with wobble angle $\theta_w = 1^\circ$. Two choices for the drag coefficient are shown, $\mathcal{R} = 10^3$ and 10^6 (left and right panel, respectively). The instability is present for all wavelengths down to λ_{min} (shaded area), despite the action of viscosity. For a wide range of core temperatures τ_{grow} is well below the precession period $P_{\text{pr}} \approx x_p P$ (we have used $P = 1$ s and $x_p = 0.1$) which is shown as a horizontal dashed line. The analytic approximations discussed in the main text are superimposed as dashed curves for the $T = 10^7$ K case. Estimates for the minima in the $T = 10^7$ K and 10^9 K curves, obtained from (77) and (78) are indicated by + symbols.

5 SUMMARY AND OUTLOOK

Within the standard two-fluid model for superfluid neutron stars we have discussed a new class of instabilities that set in through short wavelength inertial waves, provided there is sufficient relative flow along the neutron vortices. As a demonstration of the astrophysical relevance of these instabilities we have considered freely precessing neutron stars, in which the two angular velocity vectors are naturally misaligned. Our analysis is based on the usual form for the superfluid mutual friction, which depends on the strength of the drag that determines the friction between neutron vortices and the proton/electron fluid. Our results show that precession may trigger instabilities both in the weak- and strong drag regimes. Based on the analogy with the so-called Donnelly-Glaberson instability in superfluid Helium (Glaberson, Johnson & Ostermeier 1974; Barenghi, Donnelly & Vinen 2001), we argue that this instability is likely to lead to the formation of vortex tangles and generate turbulence in superfluid neutron star interiors.

The standard model (Sedrakian, Wasserman & Cordes 1999) predicts two possible precession regimes. Weak drag leads to slowly damped long period precession, while strong drag implies that precession should be fast. Assessing the stability of each precession mode we conclude that slow precession is generally stable. In particular, this should be true for the few known candidate precessors, like PSR B1828-11. An interesting exception could be slow precession of millisecond-period neutron stars. These may become unstable above a wobble angle $\theta_w \sim 1.5^\circ$ assuming a crust deformation $\epsilon \sim 5 \times 10^{-7}$, well within the theoretically allowed range (Link & Cutler 2002; Haskell et al. 2006).

In contrast, we find the fast precession solution to be unstable under generic conditions. This suggests that the solid-body rotation assumption that leads to the precession mode (Sedrakian, Wasserman & Cordes 1999) is inconsistent. The upshot of this could be that fast precession is not realised in an astrophysical system. It should certainly be the case that one cannot ignore the small scale hydrodynamical degrees of freedom in the neutron star core in an analysis of the precession problem. This is an interesting conclusion since it adds significant complexity to the modelling. It also calls into question some well established ideas.

Since the seminal discussion of Shaham (1977), it has been known that precession is sensitive to the neutron vortex dynamics. This is natural since the vortices provide the bulk of the star’s rotation. If the vortices interact strongly with the charged component (e.g. the crust) then the gyroscopic nature of the vortex array will inevitably lead to fast precession. This corresponding motion can either be described in terms of a “pinned” component affecting the usual Eulerian precession (Jones & Andersson 2001) or as a strong drag fast precession solution in the framework of Sedrakian, Wasserman & Cordes (1999). The observed long period precession of PSR B1828-11 is thus consistent only with weak mutual friction.

However, one can argue that the interaction between neutron vortices and the (much more numerous) magnetic fluxtubes in a type II proton superconductor ought to lead to strong drag (Sauls 1989; Ruderman, Zhu & Chen 1998). If this leads to the core vortices being effectively pinned to the charged component, then fast precession should result (as in the Shaham model). If on the other hand, the precession motion is able to force the vortices through the fluxtubes then the motion should be highly dissipative and there would be no lasting precession. This led Link (2003) to the suggestion that the apparent conflict with the observations can be avoided if the protons instead form a type I superconductor. There would then be no fluxtubes and slow precession may be possible. However, this would not accord with the generally held view that the protons in the outer neutron star core will condense into a type II superconductor.

Our results add yet another twist to this story. We have demonstrated that the fast precession solution, that would result if the vortices and the type II fluxtubes interact strongly, is generically unstable. Although we cannot claim to understand the dynamical repercussions of this, it seems reasonable to assume that the fast solid-body precession motion of the Sedrakian, Wasserman & Cordes (1999) model will be significantly affected. If the instability leads to a state of superfluid turbulence, as the analogy with the Helium problem suggests, then it could well be that the precession does not survive. To explore this, a meaningful analysis must venture beyond the rigid-body precession model and account for detailed superfluid hydrodynamics. This may be prohibitively difficult. Anyway, it is clear that we cannot yet use the precession observations to draw any reliable conclusions concerning the state of the proton superconductor.

The present work can (and needs to) be extended in a number of ways. Our uniform density neutron star model is too simplistic and one would certainly want to account for interior stratification etcetera. If one wants to consider superfluid-superconducting mixtures seriously then the two-fluid model probably needs to be upgraded into a more re-

alistic setup with three fluids (after relaxing the assumption of comoving charged particles), plus the magnetic field. The dynamics of such a model for neutron star cores is largely unexplored (Mendell 1998), yet the additional degrees of freedom could lead to new features. Our calculation was perturbative. Hence, little can be said about the non-linear behaviour of the unstable waves. Most likely this will be complicated, due to the small scales involved. Numerical simulations of this problem may be challenging, but should be encouraged. In fact they may be required if we are to understand the fate of a precessing neutron star in the strong-drag regime. Some of the necessary tools have already been developed by Peralta et al. (2005, 2006), and there is analogous work for superfluid Helium (Barenghi, Donnelly & Vinen 2001). Finally, at the level of linearised theory the present two-fluid analysis could be modified to consider the inner layers of the crust, where superfluid neutrons coexist with an nuclear lattice. One may expect the nature of any superfluid instabilities in that region to be different.

These are all interesting problems that we expect to return to in the future.

ACKNOWLEDGEMENTS

This work was supported by PPARC/STFC via grant number PP/E001025/1. NA also acknowledges support from PPARC via Senior Research Fellowship no PP/C505791/1.

APPENDIX A: EXPLICIT PRECESSION SOLUTIONS

We want to make quantitative contact between our local plane-wave analysis and the global motion of a freely precessing two-fluid neutron star. In particular, we need to work out the two key quantities Ω_p^{\parallel} and w_{\parallel} , which are required if we want to assess the relevance of the plane-wave instabilities.

The precession of two-fluid models, accounting for the mutual friction coupling, has been discussed by Sedrakian, Wasserman & Cordes (1999). As we will discuss in this Appendix, it is relatively straightforward to extract the information we require from their analysis. They take as their starting point the two Euler equations (1) and (2), with the mutual friction force given by (5). The precession equations are then obtained by assuming that each fluid rotates as a solid body, with the two rotation axes misaligned. The final equations of motion have a set of mode-solutions that represent free precession damped by mutual friction. Here we will briefly summarise the precession solutions in the weak and strong drag limits, and then extract the quantities Ω_p^{\parallel} and w_{\parallel} that enter into the plane-wave analysis. Having done this, we will consider an alternative approximation which allows us to extend our analysis to (essentially) the entire range of drag coefficients.

In the analysis of Sedrakian, Wasserman & Cordes (1999) it is assumed that the neutron star crust is deformed in such a way that its moment of inertia tensor has diagonal components $I_1 = I_2 = I_3/(1 + \epsilon)$, where ϵ is small. Meanwhile, the superfluid is assumed spherical and its moment of inertia is I_s . The calculation is then carried out in

the crust frame, considering perturbations around a background where $\Omega_n^i = \Omega_p^i = \Omega^i$. Assuming that the precession modes have time dependence $\exp(p\Omega t)$ one finds that p must solve

$$p^2 + \left[i(1 - \epsilon) + \tilde{I}(\mathcal{B} - i\mathcal{B}') \right] p + \epsilon(1 - \mathcal{B}' - i\mathcal{B}) = 0 \quad (\text{A1})$$

where

$$\tilde{I} = 1 + \frac{I_s}{I_1} \quad (\text{A2})$$

Once we have determined the precession period and the mutual friction damping timescale from the roots of (A1), the eigenfunctions follow from equation (74) in Sedrakian, Wasserman & Cordes (1999). This provides the relation

$$\bar{\Omega}_n = \left[1 - \frac{p}{p + i(1 - \mathcal{B}') + \mathcal{B}} \right] \bar{\Omega}_p \quad (\text{A3})$$

where we have defined

$$\bar{\Omega}_n = \Omega_{n,1} + i\Omega_{n,2}, \quad \bar{\Omega}_p = \Omega_{p,1} + i\Omega_{p,2} \quad (\text{A4})$$

and $\Omega_{n,1}$, for example, represents the \hat{x}_1 component of the angular velocity of the neutrons as measured in the crust frame.

A1 The weak drag case

In the weak drag case have $\mathcal{B} \ll 1$ and $\mathcal{B}' \approx \mathcal{B}^2$. As always, there are two mode solutions, one which corresponds to the familiar Eulerian precession of a biaxial body in the limit $\mathcal{B} \rightarrow 0$, and the other to a less familiar motion which has no analogue in one component systems. We will discuss each in turn, beginning with the Eulerian solution. To linear order in the mutual friction its frequency is given by

$$p = i\epsilon - \mathcal{B} \frac{\epsilon I_s}{(1 + \epsilon) I_1} \quad (\text{A5})$$

and the mode amplitudes in the proton and superfluid components are related by

$$\bar{\Omega}_n = \left[\frac{1}{1 + \epsilon} - \frac{i\mathcal{B}\epsilon}{(1 + \epsilon)^3} \left(1 + \epsilon + \frac{I_s}{I_1} \right) \right] \bar{\Omega}_p \quad (\text{A6})$$

Let us now assume that the eigenfunctions are normalized, i.e. choosing the precession amplitude and the initial phase, in such a way that

$$\bar{\Omega}_p = \alpha \Omega e^{p\Omega t} \quad (\text{A7})$$

with α real. Then we can immediately read off

$$\Omega_{n,1} = \alpha \Omega e^{-t/\tau_d} \cos(2\pi t/P_{\text{pr}}) \quad (\text{A8})$$

$$\Omega_{n,2} = \alpha \Omega e^{-t/\tau_d} \sin(2\pi t/P_{\text{pr}}) \quad (\text{A9})$$

where the damping time is

$$\tau_d = \frac{1}{\mathcal{B}\epsilon\Omega} \frac{I_1}{I_s} \quad (\text{A10})$$

while the precession period is

$$P_{\text{pr}} = 2\pi/\epsilon\Omega \quad (\text{A11})$$

Using (A6) we find

$$\begin{aligned} \Omega_{n,1} = & \alpha \Omega e^{-t/\tau_d} \left[\frac{1}{1 + \epsilon} \cos(2\pi t/P_{\text{pr}}) \right. \\ & \left. - \frac{\mathcal{B}\epsilon}{(1 + \epsilon)^3} \left(1 + \epsilon + \frac{I_s}{I_1} \right) \sin(2\pi t/P_{\text{pr}}) \right] \end{aligned} \quad (\text{A12})$$

$$\begin{aligned} \Omega_{n,2} = \alpha\Omega e^{-t/\tau_d} & \left[\frac{1}{1+\epsilon} \sin(2\pi t/P_{\text{pr}}) \right. \\ & \left. - \frac{\mathcal{B}\epsilon}{(1+\epsilon)^3} \left(1 + \epsilon + \frac{I_s}{I_1} \right) \cos(2\pi t/P_{\text{pr}}) \right] \quad (\text{A13}) \end{aligned}$$

It should also be recalled that we have $\Omega_{n,3} = \Omega_{p,3} = \Omega$.

We want to be able to use this solution as background for the plane-wave calculation. For this to make sense we need the rotation to be essentially constant. This is the case as long as we consider a timescale which is short compared to both the damping timescale τ_d and the precession period P_{pr} . Since \mathcal{B} is small, the strongest constraint is provided by the precession timescale. Assume that $t \ll P_{\text{pr}}$ we can use

$$\vec{\Omega}_p \approx \alpha\Omega\hat{x}_1 + \Omega\hat{x}_3 \quad (\text{A14})$$

and

$$\vec{\Omega}_n \approx \frac{\alpha\Omega}{1+\epsilon}\hat{x}_1 + \Omega\hat{x}_3 \quad (\text{A15})$$

One of the quantities we need for the plane-wave analysis is Ω_p^{\parallel} , which represents the projection of the charged component rotation along the vortex array (along Ω_n^i). To work this out we need the norm of Ω_n^i . We find that

$$\begin{aligned} \hat{n} = \frac{\vec{\Omega}_n}{\Omega_n} & \approx \\ & \approx \frac{1}{(1+\alpha^2)^{1/2}} \left(1 + \epsilon \frac{\alpha^2}{1+\alpha^2} \right) \left[\frac{\alpha}{1+\epsilon}\hat{x}_1 + \hat{x}_3 \right] \quad (\text{A16}) \end{aligned}$$

This then leads to

$$\Omega_p^{\parallel} \approx \left(1 + \epsilon \frac{\alpha^2}{1+\alpha^2} \right) \Omega_n \quad (\text{A17})$$

which shows that it is reasonable to take $\Omega_p^{\parallel} \approx \Omega_n$ in the plane-wave calculation.

We also need to estimate the relative linear velocity along the vortex array, w_{\parallel} . We obtain this quantity from

$$w_{\parallel} = (v_n^i - v_p^i)\hat{n}_i \quad (\text{A18})$$

where

$$v_x^i = \epsilon^{ijk}\Omega_j^x x_k \quad (\text{A19})$$

In other words, the frame independent scalar quantity that we need follows from

$$w_{\parallel} = \epsilon^{ijk}\hat{n}_i(\Omega_j^n - \Omega_j^p)x_k \quad (\text{A20})$$

From our mode solutions we find

$$\vec{\Omega}_n - \vec{\Omega}_p \approx -\frac{\alpha\epsilon\Omega}{1+\epsilon}\hat{x}_1 \quad (\text{A21})$$

Then

$$(\vec{\Omega}_n - \vec{\Omega}_p) \times \hat{n} \approx \frac{\epsilon\alpha\Omega}{(1+\alpha^2)^{1/2}} \left[1 + \frac{\epsilon\alpha^2}{1+\alpha^2} \right] \hat{x}_2 \quad (\text{A22})$$

and we see that

$$w_{\parallel} \approx \epsilon\alpha\Omega x_2 \quad (\text{A23})$$

Finally, we would like to be able to make direct contact with observations. This involves working out the ‘‘wobble angle’’ θ_w associated with our precession solution. As in the analysis of Jones & Andersson (2001), we define the wobble angle to be the angle between the total angular momentum axis and the crust deformation axis. In the present case the

latter is simply \hat{x}_3 . Meanwhile, in the crust frame, the total angular momentum is given by

$$\vec{J} = (I_1\Omega_1^p + I_s\Omega_1^n)\hat{x}_1 + (I_1\Omega_2^p + I_s\Omega_2^n)\hat{x}_2 + (I_3 + I_s)\Omega\hat{x}_3 \quad (\text{A24})$$

Taking the modulus of this, we then find the wobble angle from

$$\vec{J} \cdot \hat{x}_3 = (I_3 + I_s)\Omega = J \cos\theta_w \quad (\text{A25})$$

In the weak drag case we then have

$$J \approx (I_s + I_3)\Omega \left[1 + \frac{\alpha^2}{2(1+\epsilon)^2} \right] \quad (\text{A26})$$

Hence

$$\theta_w \approx \frac{\alpha}{1+\epsilon} \approx \alpha \quad (\text{A27})$$

This completes our analysis of the motion associated with (A5).

We now turn to the second mode found for weak mutual friction. Its frequency is given by

$$p = -i - \mathcal{B} \frac{\tilde{I} + \epsilon}{1 + \epsilon}, \quad (\text{A28})$$

while the superfluid and proton mode amplitudes are related by

$$\bar{\Omega}_p = i\mathcal{B} \frac{I_s}{I_3} \bar{\Omega}_n. \quad (\text{A29})$$

To gain insight as to what sort of motion this mode corresponds to, consider the case $\mathcal{B} = 0$. Then we can write

$$\bar{\Omega}_p = 0, \quad (\text{A30})$$

$$\bar{\Omega}_n = \alpha\Omega, \quad (\text{A31})$$

i.e. the crust is unperturbed, and keeps spinning at a rate Ω about the inertial 3-axis, but the superfluid does something more complicated. Writing the superfluid components explicitly, we have

$$\Omega_{n,1} = \alpha\Omega \cos(\Omega t), \quad (\text{A32})$$

$$\Omega_{n,2} = -\alpha\Omega \sin(\Omega t). \quad (\text{A33})$$

It is then straightforward to show that the rate of change of $\bar{\Omega}_n$ with respect to the *inertial frame* is zero:

$$\frac{d\Omega_{n,i}}{dt_I} = \frac{d\Omega_{n,i}}{dt_R} + \epsilon_{ijk}\Omega^j\Omega_n^k = 0, \quad (\text{A34})$$

where the subscripts ‘I’ and ‘R’ label time derivatives in the inertial and rotating frames, respectively. It follows that the superfluid’s angular velocity is fixed in space; in this limit the mode corresponds to a misalignment between the crust and superfluid spin axes by an angle α . The relative velocity between the crust and superfluid is then

$$w_i = \epsilon_{ijk}\Omega_n^j x^k, \quad (\text{A35})$$

which gives a relative flow along the vortices at time $t = 0$ of

$$w_{\parallel} = x_2\alpha\Omega. \quad (\text{A36})$$

This remains true to leading order in the case of small but non-zero \mathcal{B} .

When $\mathcal{B} \neq 0$ we instead have

$$\Omega_{n,1} = \alpha\Omega \cos(\Omega t)e^{-t/\tau_d}, \quad (\text{A37})$$

$$\Omega_{n,2} = -\alpha\Omega \sin(\Omega t)e^{-t/\tau_d}, \quad (\text{A38})$$

$$\Omega_{p,1} = \alpha\Omega\mathcal{B}\frac{I_s}{I_3} \sin(\Omega t)e^{-t/\tau_d}, \quad (\text{A39})$$

$$\Omega_{p,2} = \alpha\Omega\mathcal{B}\frac{I_s}{I_3} \cos(\Omega t)e^{-t/\tau_d}, \quad (\text{A40})$$

where the damping time τ_d is given by

$$\tau_d = \frac{1}{\mathcal{B}\Omega} \frac{1+\epsilon}{\tilde{I}+\epsilon}. \quad (\text{A41})$$

The total angular momentum is the sum of the neutron and proton contributions, which can be shown to be given by

$$J_1 = \alpha\Omega e^{-t/\tau_d} I_s \cos\left[\Omega t - \frac{\mathcal{B}}{1+\epsilon}\right], \quad (\text{A42})$$

$$J_2 = -\alpha\Omega e^{-t/\tau_d} I_s \sin\left[\Omega t - \frac{\mathcal{B}}{1+\epsilon}\right], \quad (\text{A43})$$

$$J_3 = I_3\Omega. \quad (\text{A44})$$

From these equations we can easily compute the angle between J_i and the crust's 3-axis:

$$\cos^{-1}(\hat{J} \cdot \hat{x}_3) = \alpha e^{-t/\tau_d} \frac{I_s}{I_s + I_3}. \quad (\text{A45})$$

The constancy of this angle (aside from its slow monotonic decrease) shows that the crust's 3-axis moves on a cone about the fixed total angular momentum. To see exactly how the body moves it is best to make use of Euler angles (θ, ϕ, ψ) giving the orientation of the body axes with respect to some fixed inertial axes. Then the angular velocity components of the crust referred to the rotating crust frame take the form, see e.g. Landau & Lifshitz (1976),

$$\Omega_{p,1} = \dot{\phi} \sin \theta \sin \psi + \dot{\theta} \cos \psi, \quad (\text{A46})$$

$$\Omega_{p,2} = \dot{\phi} \sin \theta \cos \psi - \dot{\theta} \sin \psi, \quad (\text{A47})$$

$$\Omega_{p,3} = \dot{\phi} \cos \theta + \dot{\psi}. \quad (\text{A48})$$

In defining (θ, ϕ, ψ) we are free to make any choice of fixed inertial frame we want, but obviously it would be simplest to choose one where the inertial 3-axis of this system lies along the fixed angular momentum vector. Then $\theta = \cos^{-1}(\hat{J} \cdot \hat{x}_3)$ which is a constant, so the above equations reduce to

$$\Omega_{p,1} = \dot{\phi} \sin \theta \sin \psi, \quad (\text{A49})$$

$$\Omega_{p,2} = \dot{\phi} \sin \theta \cos \psi, \quad (\text{A50})$$

$$\Omega_{p,3} = \dot{\phi} \cos \theta + \dot{\psi}, \quad (\text{A51})$$

where

$$\theta = \alpha e^{-t/\tau_d} \frac{I_s}{I_s + I_3}. \quad (\text{A52})$$

Now compare with

$$\Omega_{p,1} = A \sin \Omega t, \quad (\text{A53})$$

$$\Omega_{p,2} = A \cos \Omega t, \quad (\text{A54})$$

$$\Omega_{p,3} = \Omega, \quad (\text{A55})$$

where

$$A = \alpha\Omega e^{-t/\tau_d} \mathcal{B} \frac{I_s}{I_3}. \quad (\text{A56})$$

It follows at once that

$$A^2 = \dot{\phi}^2 \theta^2 \Rightarrow \dot{\phi} = \Omega \mathcal{B} \frac{I_s + I_3}{I_3}, \quad (\text{A57})$$

and the $\Omega_{p,3}$ equation gives

$$\dot{\psi} = \Omega - \dot{\phi} = \Omega \left[1 - \mathcal{B} \frac{I_s + I_3}{I_3}\right]. \quad (\text{A58})$$

Collecting results:

$$\theta = \alpha e^{-t/\tau_d} \frac{I_s}{I_s + I_3} \sim \text{constant}, \quad (\text{A59})$$

$$\dot{\phi} = \mathcal{B}\Omega \frac{I_s + I_3}{I_3} \ll \Omega, \quad (\text{A60})$$

$$\dot{\psi} = \Omega \left[1 - \mathcal{B} \frac{I_s + I_3}{I_3}\right] \approx \Omega. \quad (\text{A61})$$

We therefore see that the motion is still rather simple, with the crust's 3-axis moving in a cone of half-angle θ about the fixed angular momentum axis at the slow rate $\dot{\phi} \ll \Omega$, with a rapid rotation at rate $\dot{\psi} \approx \Omega$ about the crust's 3-axis superimposed.

Amusingly, this is the opposite of normal free precession, i.e. small angle free precession of a single component rigid biaxial (but nearly spherical) body, as in that case $\dot{\phi} \approx \Omega$ and $|\dot{\psi}| \approx \epsilon\Omega \ll \Omega$. However, from the point of view of the radio observations, both sorts of precession consist of two superimposed rotations misaligned by a small angle and so are observationally indistinguishable. This means that rather than interpreting PSR1828-11 as undergoing the usual precession mode with the ratio $P/P_{\text{pr}} \sim \epsilon$, we would instead have

$$\frac{P}{P_{\text{pr}}} \approx \frac{\dot{\phi}}{\dot{\psi}} \approx \mathcal{B} \frac{I_s + I_3}{I_3} \quad (\text{A62})$$

The potential physical significance of this is discussed in Section 4.1.

A2 The strong drag case

In the strong drag limit we have $\mathcal{B} \ll 1$ and $1 - \mathcal{B}' \approx \mathcal{B}^2$. In this case we find the two precession modes

$$p = -\frac{\epsilon}{\bar{\sigma}} [i(1 - \mathcal{B}') + \mathcal{B}] \quad (\text{A63})$$

a mode which damps out before it completes one full cycle, and

$$p = i\bar{\sigma} - \mathcal{B} \frac{1 + \bar{\sigma}}{\bar{\sigma}} \frac{I_s}{I_1} \quad (\text{A64})$$

In these expressions we have used

$$\bar{\sigma} = \epsilon + \frac{I_s}{I_1} \quad (\text{A65})$$

The solution (A64) represents slowly damped fast precession, since $I_s/I_1 \sim 10 \gg \epsilon$. This is essentially the precession mode discovered by Shaham (1977) for a neutron star model where an amount I_s of neutron vortices is perfectly pinned.

Focusing on (A64) we find that the damping time is

$$\tau_d = \frac{\bar{\sigma}}{\mathcal{B}\Omega(1 + \bar{\sigma})} \frac{I_1}{I_s} \quad (\text{A66})$$

while the precession period is

$$P_{\text{pr}} = \frac{2\pi}{\bar{\sigma}\Omega} \quad (\text{A67})$$

As in the weak coupling case the damping is relatively slow.

The amplitudes are related by

$$\bar{\Omega}_n = -i\frac{\mathcal{B}}{\bar{\sigma}}\bar{\Omega}_p = -i\mathcal{B}\left(\epsilon + \frac{I_s}{I_1}\right)^{-1}\bar{\Omega}_p \quad (\text{A68})$$

Again assuming that the plane-wave analysis is relevant on a timescale short compared to P_{pr} , we find the approximate mode solution

$$\bar{\Omega}_p \approx \alpha\Omega\hat{x}_1 + \Omega\hat{x}_3 \quad (\text{A69})$$

$$\bar{\Omega}_n \approx -\alpha\mathcal{B}\Omega\left(\epsilon + \frac{I_s}{I_1}\right)^{-1}\hat{x}_2 + \Omega\hat{x}_3 \quad (\text{A70})$$

In this case we see that

$$\hat{n} \approx -\alpha\mathcal{B}\left(\epsilon + \frac{I_s}{I_1}\right)^{-1}\hat{x}_2 + \hat{x}_3 \quad (\text{A71})$$

and it immediately follows that

$$\Omega_p^{\parallel} \approx \Omega_n \quad (\text{A72})$$

as before.

To work out the relative flow along the vortex array, we take the same steps as in the weak drag case. This leads to

$$\bar{\Omega}_n - \bar{\Omega}_p \approx -\alpha\Omega\hat{x}_1 - \alpha\mathcal{B}\Omega\left(\epsilon + \frac{I_s}{I_1}\right)^{-1}\hat{x}_2 \quad (\text{A73})$$

and

$$\begin{aligned} (\bar{\Omega}_n - \bar{\Omega}_p) \times \hat{n} &\approx -\alpha\mathcal{B}\Omega\left(\epsilon + \frac{I_s}{I_1}\right)^{-1}\hat{x}_1 \\ &+ \alpha\Omega\hat{x}_2 - \alpha^2\mathcal{B}\Omega\left(\epsilon + \frac{I_s}{I_1}\right)^{-1}\hat{x}_3 \end{aligned} \quad (\text{A74})$$

which means that

$$w_{\parallel} \approx \alpha\Omega x_2 \quad (\text{A75})$$

The final step again concerns the wobble angle. For the above solution we find that

$$J \approx (I_s + I_3)\Omega\left[1 + \frac{\alpha^2 I_1^2}{2(I_s + I_3)^2}\right] \quad (\text{A76})$$

which leads to

$$\theta_w \approx \frac{\alpha I_1}{I_s + I_3} \approx \frac{\alpha I_1}{I_s} \quad (\text{A77})$$

since $\epsilon \ll I_s/I_1$

A3 The ‘‘general’’ case

So far, the precession solutions that we have discussed are identical to the limiting cases considered by Sedrakian, Wasserman & Cordes (1999). However, we can do better than this and find solutions that are valid across the range of permissible drag coefficients, \mathcal{R} . The starting point is (A1) as before, but now we assume that ϵ is the small parameter. This approximation is generally valid as long as $\mathcal{B} \gg \epsilon$, i.e. it fails only in the extreme weak drag limit (which we have already analyzed above).

Considering (A1) to order ϵ we find the two solutions

$$p_1 \approx -\epsilon \frac{1 - \mathcal{B}' - i\mathcal{B}}{i(1 - \tilde{I}\mathcal{B}') + \tilde{I}\mathcal{B}} \quad (\text{A78})$$

and

$$p_2 \approx -\tilde{I}\mathcal{B} - i\left(1 - \tilde{I}\mathcal{B}'\right) + \epsilon \frac{I_s}{I_1} \frac{i\mathcal{B} + \mathcal{B}'}{i(1 - \tilde{I}\mathcal{B}') + \tilde{I}\mathcal{B}} \quad (\text{A79})$$

It is quite straightforward to show that these solution behave in the anticipated way in the weak- and strong drag limits. In particular, we find that (A78) limits to (A5) when $\mathcal{R} \rightarrow 0$ and to (A63) for $\mathcal{R} \rightarrow \infty$. Meanwhile, (A79) reduces to (A28) and to (A64) in the respective limits.

To extract the precession period and the damping time we need the real and imaginary parts of p . The first solution (A78) can be written

$$p_1 \approx -\frac{\epsilon}{\mathcal{D}} \left\{ -(1 - \tilde{I})\mathcal{B} - i \left[\tilde{I}\mathcal{B}^2 + (1 - \mathcal{B}')(1 - \tilde{I}\mathcal{B}') \right] \right\} \quad (\text{A80})$$

where we have introduced

$$\mathcal{D} = \tilde{I}^2\mathcal{B}^2 + (1 - \tilde{I}\mathcal{B}')^2 \quad (\text{A81})$$

Since we assume that the perturbations behave as $e^{p\Omega t}$ we see that the damping time is

$$\tau_d \approx \frac{\mathcal{D}}{(\tilde{I} - 1)\epsilon\mathcal{B}\Omega} \quad (\text{A82})$$

while the precession period is

$$P_{\text{pr}} \approx \frac{2\pi}{\epsilon\Omega} \frac{\mathcal{D}}{\tilde{I}\mathcal{B}^2 + (1 - \mathcal{B}')(1 - \tilde{I}\mathcal{B}')} \quad (\text{A83})$$

Given the above estimates we can determine the parameter range for which this precession mode is relevant. A reasonable criterion would be that the precession motion does not damp out before a single cycle is completed. This means that we must have $\tau_d/P_{\text{pr}} < 1$. For the solution given above we find that this is true provided that

$$\mathcal{R} < \frac{1}{2\pi} \frac{I_1}{I_s} \approx 0.016 \quad (\text{A84})$$

for our canonical parameters, cf. the left panel of Figure A1. For larger values of the drag coefficient this solution is overdamped. Since the maximum value of \mathcal{R} that we need to consider is small, one would expect the weak drag estimate to be sufficiently accurate for our analysis. As we can see in Figure A1 the weak drag solution matches the exact result well even before \mathcal{R} enters the range (A84).

Let us now move on to the second precession solution, (A79). Here the algebra gets a little bit messier. The frequency is given by

$$p_2 \approx -\tilde{I}\mathcal{B} + \epsilon \frac{I_s\mathcal{B}}{I_1\mathcal{D}} - i \left\{ (1 - \tilde{I}\mathcal{B}') - \epsilon \frac{I_s}{I_1\mathcal{D}} \left[\tilde{I}\mathcal{B}^2 - (1 - \tilde{I}\mathcal{B}')\mathcal{B}' \right] \right\} \quad (\text{A85})$$

from which we see that the precession period is

$$P_{\text{pr}} \approx -\frac{2\pi}{(1 - \tilde{I}\mathcal{B}')\Omega} \left[1 + \frac{\epsilon I_s}{I_1\mathcal{D}} \frac{\tilde{I}\mathcal{B}^2 - (1 - \tilde{I}\mathcal{B}')\mathcal{B}'}{1 - \tilde{I}\mathcal{B}'} \right] \quad (\text{A86})$$

Meanwhile, the damping timescale is

$$\tau_d \approx \frac{1}{\tilde{I}\Omega\mathcal{B}} \left(1 + \epsilon \frac{I_s}{I_1\tilde{I}\mathcal{D}} \right) \quad (\text{A87})$$

Again, we can assess the relevance of this mode by checking that it is not overdamped. The behaviour is illustrated in the right panel of Figure A1. In this case we find acceptable solution for

$$\mathcal{R} > 2\pi \left(1 + \frac{I_1}{I_s} \right) \approx 7 \quad (\text{A88})$$

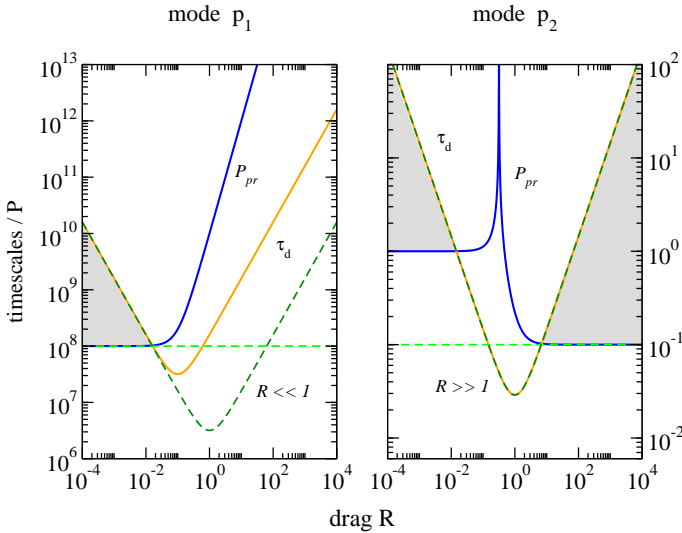


Figure A1. The solutions $\{P_{pr}, \tau_d\}$ for the precession modes p_1 (left panel) and p_2 (right panel) for a general mutual friction drag \mathcal{R} . These are compared to the weak and strong drag solutions, left and right panel respectively, represented by the dashed curves. The shaded areas correspond to the intervals of \mathcal{R} for which precession is not overdamped by mutual friction, i.e., $\tau_d > P_{pr}$. Note that all timescales are normalised with the rotational period P .

In this case \mathcal{R} is sufficiently large (compared to unity) that one would expect the strong drag approximation to give reliable results. Indeed, it is clear from Figure A1 that one would expect the strong drag approximation to be valid when this mode is oscillatory. In addition, the figure shows that the mode is also relevant for $\mathcal{R} < 0.01$. In that regime it is well approximated by the weak-drag solution (A28).

In practice, the results for the general precession modes, p_1 and p_2 , shows that the (much simpler) approximate weak and strong drag solutions apply for the entire range of \mathcal{R} for which precession is not overdamped.

REFERENCES

- Abney, M., Epstein, R.I., Olinto, A.V., 1996, Ap. J. Lett. **466**, L91
 Akgün, T., Link B., Wasserman, I., 2006, MNRAS **365**, 653
 Alpar, M.A., Langer, S.A., Sauls, J.A., 1984, Ap. J., **282** 533
 Alpar, M. A., Sauls, J. A., 1988, Ap. J. **327**, 723
 Andersson, N., Comer, G.L., 2006, Class. Quantum Grav. **23** 5505
 Andersson, N., Comer, G.L., Glampedakis, K., 2005, Nucl. Phys. A **763**, 212
 Andersson, N., Comer, G.L., Prix, R., 2004, MNRAS **354** 101
 Andersson, N., Sidery, T., Comer G.L., 2006, MNRAS **368**, 162
 Andersson, N., Sidery, T., Comer, G.L., 2007, MNRAS **381**, 747
 Barenghi, C.F., Donnelly, R.J., Vinen W.F., 2001, *Quantized Vorticity and Superfluid Turbulence* (Springer, Heidelberg)

- Baym, G., Pethick, C., Pines, D., 1969, Nature **224**, 673
 Cutler, C., Ushomirsky, G., Link, B., 2003, Ap. J. **588**, 975
 Flowers, E., Itoh, N., 1976, Ap. J. **206**, 218
 Glaberson, W. I., Johnson, W.W., Ostermeier, R.M., 1974, Phys. Rev. Lett., **33** 1197
 Glampedakis, K., Andersson, N., Jones, D.I., 2007, *On the stability of precessing superfluid neutron stars* preprint arXiv:0708.2693
 Haberl et al., 2006, Astron. Astrophys. **451**, L17
 Hall, H.E., Vinen, W.F., 1956, Proc. R. Soc. London A **238**, 215
 Haskell, B., Jones, D.I., Andersson, N., 2006, MNRAS **373** 1423
 Jones, D.I., Andersson, N., 2001, MNRAS **324**, 811
 Landau, L.D., Lifshitz, E.M., 1976, *Mechanics* (Butterworth-Heinemann)
 Link, B., 2003, Phys. Rev. Lett., **91**, 101101
 Link B., 2006, Astron. Astrophys. **458**, 881
 Link, B., Cutler, C., 2002, MNRAS, **336**, 211
 Link, B., Epstein, R.I., 2001, Ap. J. **556**, 392
 Mendell, G., 1998, MNRAS **296**, 903
 Middleditch J., et al. 2000, *New Astronomy* **5** no. 5, 243
 Middleditch J., et al. 2000, astro-ph/0010044
 Peralta, C., Melatos, A., Giacobello, M., Ooi, A., 2005, Ap. J. **635** 1224
 Peralta, C., Melatos, A., Giacobello, M., Ooi, A., 2006, Ap. J. **651** 1079
 Ruderman, M., Zhu, T., Chen, K., 1998, Ap. J, **492**, 267
 Sauls, J.A., 1989, in *Timing Neutron stars*, ed. Ogelman H. and van de Heuvel E.P.J. (Kluwer Academic Publishers)
 Sedrakian, A., Wasserman, I., Cordes, J.M., 1999, Ap. J. **524**, 341
 Shabanova, T., Lyne, A.G., Urama, J.O., 2001, Ap. J. **552**, 321
 Shaham, J., 1977, Ap. J. **214**, 251
 Sidery, T., Andersson, N., Comer, G.L., 2007, to appear in MNRAS (preprint astro-ph/0706.0672)
 Sonin, E.B., 1987, Rev. Mod. Phys. **59**, 87
 Stairs, I.H., Lyne, A.G., Shemar, S.L., 2000, Nature **406**, 484